arXiv:1412.3994v1 [cond-mat.mes-hall] 12 Dec 2014

Photon-assisted electronic and spin transport through a precessing single-molecule magnet

Milena Filipović[1] and Wolfgang Belzig[1]

[1] *Fachbereich Physik, Universität Konstanz, D-78457 Konstanz, Germany*

(Dated: December 15, 2014)

We study the ac-charge and -spin transport through an orbital of a single molecule magnet precessing in a constant magnetic field. We assume that the source and drain contacts have time-dependent chemical potentials. We employ the Keldysh Green's functions method to calculate the spin and charge currents to linear order in the time-dependent potentials. The molecular and electronic spins are coupled via exchange interaction. The time-dependent molecular spin drives inelastic transitions between the Zeeman split orbital energy levels resulting in a rich structure in the transport characteristics. The time-dependent voltages allow to reveal the internal precession time scale (the Larmor frequency) by a dc-conductance measurement if the ac-frequency matches the Larmor frequency. Furthermore we show that the setup can be used to generate dc-spin currents with arbitrary magnetization direction by controlling the relative phases between the Larmor precession and the ac-voltage.

PACS numbers: 73.23.-b, 75.76.+j, 85.65.+h, 85.75.-d

I. INTRODUCTION

Already decades ago the potential use of molecules as components of electronic circuitry was proposed[1] thereby introducing the field of molecular electronics. Since then, the goal of the field has been to create high-speed processing molecular devices with miniature size.[2,3] In that respect it is important to investigate the properties of transport through single molecules in the presence of external fields.[4–8] Single-molecule magnets (SMMs) are a class of molecules with a permanent magnetization. Due to both classical[9] and quantum[9–12] characteristics of SMMs, their application in molecular electronics became a topic of intense research considering their potential usage in creation of memory devices.[13]

Time-dependent transport through molecular junctions has been theoretically studied using different techniques, such as nonequilibrium Green's functions technique,[14–18] time-dependent density functional theory,[19–23] reduced density matrix approach,[24] etc. Time-dependent periodic fields in electrical contacts cause photon-assisted tunneling,[4,25–27] a phenomenon based on the fact that by applying an external harmonic field with frequency Ω to the contact, the conduction electrons interact with the ac field and consequently participate in the inelastic tunneling processes by absorbing or emitting an amount of energy $n\hbar\Omega$, where $n \in \mathbb{Z}^*$. Theoretically, photon-assisted tunneling through atoms and molecules was investigated in numerous works.[4,28–33] Some experimental studies addressed photon-assisted tunneling through atomic-sized[34–36] and molecular[37,38] junctions in the presence of laser fields. In junctions with time-dependent ac bias the presence of displacement currents is inevitable due to the charge accumulation in the scattering region.[39,40] This problem can be solved either implicitly by including the Coulomb interaction in the Hamiltonian of the system,[41,42] or explicitly by adding the displacement current to the conduction current,[40,43] thus providing the conservation of the total ac current.

Spin transport through magnetic nanostructures can be used to manipulate the state of the magnetization via spin-transfer torques (STTs).[44,45] The concept of STT is based on the transfer of spin angular momenta from the conduction electrons to a local magnetization in the scattering region generating a torque as a back-action of the spin transport and thus changing the state of the magnetic nanostructure.[44–47] Hence, current-induced magnetization reversal became an active topic in recent years.[48–54] The measurement and control of the magnetization of SMMs[55] employing spin transport may bring important applications in spintronics.

In this work we theoretically study the charge and spin transport through a single electronic energy level in the presence of a precessing SMM, in a constant magnetic field. The electronic level may be an orbital of the SMM, or it may belong to a nearby quantum dot. The SMM precesses with the Larmor frequency ω_L around the magnetic field axis. Its spin is treated as a classical magnetic moment. The Zeeman splitting and interaction of the orbital with the precessing SMM result in four (quasi-)energy levels in the quantum dot. The system is then connected to electric contacts subject to oscillating electric potentials with frequency Ω, which are considered as a perturbation. The oscillating chemical potentials induce photon-assisted charge and spin tunneling. In the limit of low ac frequency this junction can be mapped onto an effective electric circuit. The dynamic conductance associated with the resonant position of the chemical potentials with (quasi-)energy levels in the molecular orbital, is enhanced for $\Omega = \omega_L$. A photon-assisted STT is exerted on the molecular spin by the photon-assisted spin-currents. The precessing molecular spin in turn pumps spin-currents. The in-plane x and y photon-assisted spin-current components oscillate with frequency

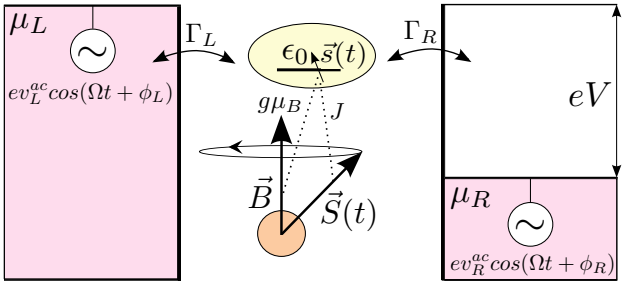

FIG. 1: (Color online) Photon-assisted tunneling through a single molecular level with energy ϵ_0 coupled to the spin $\vec{S}$ of a single-molecule magnet via exchange interaction with the coupling constant J, in the presence of a constant magnetic field $\vec{B}$. External ac potentials $V_{\rm ac}^{\xi}(t) = v_{\rm ac}^{\xi} cos(\Omega t + \phi_\xi)$ are applied to the leads $\xi = L, R$ with chemical potentials μ_ξ and tunnel rates Γ_ξ.

$2\omega_L$ in the case $\Omega = \omega_L$, and have nonzero time-averaged contributions. Their directions and magnitudes are controllable by tuning the phases of the ac fields in the leads. A part of this article is a complement to Ref. 56, representing the solution for the Gilbert damping coefficient[57] non-perturbative in the coupling to the SMM in the absence of time-varying voltage. The other corresponding STT coefficients, and an arising nonzero z-component of the STT are obtained as well.

The article is organized in the following way: We describe the model setup of the system in Sec. II. The theoretical formalism based on the Keldysh nonequilibrium Green's functions technique[14–16] is introduced in Sec. III. Here we derive expressions for spin and charge currents in linear order with respect to ac harmonic potentials in the leads. In Sec. IV we obtain and analyze the dynamic conductance of the charge current using the current partitioning scheme developed by Wang *et al.*[43] This section is followed by Sec. V in which we analyze resonant and photon-assisted spin transport and STT. We finally conclude in Sec. VI.

II. MODEL SETUP

We consider a junction consisting of a single spin-degenerate molecular orbital of a precessing SMM in a constant magnetic field along z-axis, $\vec{B} = B\vec{e}_z$, coupled to two normal metallic leads. We assume the spin of the SMM is large enough so that we can neglect the quantum fluctuations and treat it as a classical vector $\vec{S}$, with constant length $S = |\vec{S}|$. The magnetic field does not affect the electric contacts, which are assumed to be noninteracting. An external ac harmonic potential $V_{\rm ac}^{\xi}(t) = v_{\rm ac}^{\xi} cos(\Omega t + \phi_\xi)$ is applied to each lead $\xi = L, R$, modulating the single electron energy as $\epsilon_{k\sigma\xi}(t) = \epsilon_{k\sigma\xi} + eV_{\rm ac}^{\xi}(t)$, with $\epsilon_{k\sigma\xi}$ being the single-particle energy of an electron with the wave number k, in the absence of the time-varying voltage [see Fig. 1]. The subscript $\sigma = \uparrow, \downarrow = 1, 2 = \pm 1$ denotes the spin-up or spin-down state of the electrons. Since we want to unravel the quantum effects induced by the tunneling electrons and the ac harmonic potentials, we consider a well coupled molecular orbital and treat it as noninteracting by disregarding the intra-orbital Coulomb interactions between the electrons.

The junction is described by the Hamiltonian $\hat{H}(t) = \hat{H}_L(t) + \hat{H}_R(t) + \hat{H}_T + \hat{H}_{MO}(t) + \hat{H}_S$. Here $\hat{H}_\xi(t) = \sum_{k,\sigma} \epsilon_{k\sigma\xi}(t) \hat{c}^\dagger_{k\sigma\xi} \hat{c}_{k\sigma\xi}$ is the Hamiltonian of lead $\xi = L, R$. The tunneling Hamiltonian $\hat{H}_T = \sum_{k,\sigma,\xi} [V_{k\xi} \hat{c}^\dagger_{k\sigma\xi} \hat{d}_\sigma + V^*_{k\xi} \hat{d}^\dagger_\sigma \hat{c}_{k\sigma\xi}]$ introduces the spin-independent tunnel coupling between the molecular orbital and the leads, with matrix element $V_{k\xi}$. The operators $\hat{c}^\dagger_{k\sigma\xi}(\hat{c}_{k\sigma\xi})$ and $\hat{d}^\dagger_\sigma(\hat{d}_\sigma)$ represent the creation (annihilation) operators of the electrons in the leads and the molecular orbital. The next term in the Hamiltonian of the system is given by $\hat{H}_{MO}(t) = \sum_\sigma \epsilon_0 \hat{d}^\dagger_\sigma \hat{d}_\sigma + (g\mu_B/\hbar)\hat{\vec{s}}\vec{B} + J\hat{\vec{s}}\vec{S}(t)$. Here, the first term describes the noninteracting molecular orbital with energy ϵ_0. The second and third terms represent the interactions of the electronic spin $\hat{\vec{s}} = (\hbar/2) \sum_{\sigma\sigma'} (\hat{\vec{\sigma}})_{\sigma\sigma'} \hat{d}^\dagger_\sigma \hat{d}_{\sigma'}$ in the molecular orbital with the external constant magnetic field $\vec{B}$ and the molecular spin $\vec{S}(t)$. Here, $\hat{\vec{\sigma}} = (\hat{\sigma}_x, \hat{\sigma}_y, \hat{\sigma}_z)^T$ represents the vector of the Pauli matrices. The proportionality factors g and μ_B are the gyromagnetic ratio of the electron and the Bohr magneton, respectively, while J is the exchange coupling constant between the molecular and electronic spins.

Presuming for simplicity that the molecular spin g-factor equals that of a free electron, the last term in the Hamiltonian of the junction $\hat{H}_S = g\mu_B \vec{S}\vec{B}$ represents the interaction between the molecular spin $\vec{S}$ and the magnetic field $\vec{B}$. Accordingly $\hat{H}_S$ does not affect the charge and spin transport, but contributes to the spin dynamics of the SMM, in such a way that the molecular spin precesses around the magnetic field axis. Since we assume the molecular magnet spin to be classical the dynamics is given by $\vec{S}(t) = S_\perp \cos(\omega_L t)\vec{e}_x + S_\perp \sin(\omega_L t)\vec{e}_y + S_z \vec{e}_z$, where $S_\perp$ is the magnitude of the instantaneous projection of $\vec{S}(t)$ onto the xy plane, given by $S_\perp = S\sin(\theta)$, while the projection of the molecular spin on the z-axis equals $S_z = S\cos(\theta)$. Here θ is the angle between $\vec{B}$ and $\vec{S}(t)$, and $\omega_L = g\mu_B B/\hbar$ is the Larmor precession frequency. To compensate for the dissipation of magnetic energy due to the interaction with conduction electrons, we assume that the molecular spin is kept precessing by external means (e.g., rf fields).[58] Hence, we keep the tilt angle θ fixed and determined by the initial conditions.

III. THEORETICAL FORMALISM

The ensemble and quantum average charge and spin currents from the lead ξ to the molecular orbital are given

by

$$I_{\xi\nu}(t) = q_\nu \left\langle \frac{d}{dt}\hat{N}_{\xi\nu} \right\rangle = q_\nu \frac{i}{\hbar}\big\langle [\hat{H}, \hat{N}_{\xi\nu}] \big\rangle, \qquad (1)$$

with $\hat{N}_{\xi\nu} = \sum_{k,\sigma,\sigma'} \hat{c}^\dagger_{k\sigma\xi}(\hat{\sigma}_\nu)_{\sigma\sigma'}\hat{c}_{k\sigma'\xi}$ representing the charge and spin occupation number operator of the contact ξ. The index ν takes values $\nu = 0$ for the charge and $\nu = 1, 2, 3$ for the components x, y, z of the spin-polarized current. The prefactors q_ν correspond to the electronic charge $q_0 = -e$ and spin $q_{\nu\neq 0} = \hbar/2$. Employing the Keldysh nonequilibrium Green's functions technique, the currents can be calculated in units in which $\hbar = e = 1$ as[15,16]

$$I_{\xi\nu}(t) = -2q_\nu \mathrm{Re}\int dt' \mathrm{Tr}\big\{\hat{\sigma}_\nu[\hat{G}^r(t,t')\hat{\Sigma}^<_\xi(t',t) + \hat{G}^<(t,t')\hat{\Sigma}^a_\xi(t',t)]\big\}, \qquad (2)$$

where $\hat{\sigma}_0 = \hat{1}$ is the identity operator, while $\hat{\sigma}_{\nu\neq 0}$ are Pauli operators. In Eq. (2), $\hat{\Sigma}^{r,a,<}_\xi(t,t')$ are the retarded, advanced, and lesser self-energies from the tunnel coupling between the molecular orbital and the lead ξ, while $\hat{G}^{r,a,<}(t,t')$ are the corresponding Green's functions of the electrons in the molecular orbital. The matrices of the self-energies are diagonal in the electronic spin space with respect to the basis of eigenstates of $\hat{s}_z$, and their nonzero entries are given by $\Sigma^{r,a,<}_\xi(t,t') = \sum_k V_{k\xi} g^{r,a,<}_{k\xi}(t,t')V^*_{k\xi}$, where $g^{r,a,<}_{k\xi}(t,t')$ are the retarded, advanced and lesser Green's functions of the electrons in contact ξ. The matrix elements of the Green's functions $\hat{G}^{r,a,<}(t,t')$ are given by $G^{r,a}_{\sigma\sigma'}(t,t') = \mp i\theta(\pm t \mp t')\langle\{\hat{d}_\sigma(t), \hat{d}^\dagger_{\sigma'}(t')\}\rangle$ and $G^<_{\sigma\sigma'}(t,t') = i\langle \hat{d}^\dagger_{\sigma'}(t')\hat{d}_\sigma(t)\rangle$, where $\{\cdot,\cdot\}$ denotes the anticommutator. The self-energies of lead ξ can be expressed as[14–16]

$$\Sigma^<_\xi(t,t') = i\int \frac{d\epsilon}{2\pi} e^{-i\epsilon(t-t')+i\varphi^\xi(t,t')} f_\xi(\epsilon)\Gamma_\xi(\epsilon),$$
$$\Sigma^r_\xi(t,t') = -i\theta(t-t')\int \frac{d\epsilon}{2\pi} e^{-i\epsilon(t-t')+i\varphi^\xi(t,t')}\Gamma_\xi(\epsilon)\,.$$

Here we introduced the Faraday phases $\varphi^\xi(t,t') = e\int_t^{t'} dt'' V^\xi_{ac}(t'')$. From its definition it follows that $\Sigma^a_\xi(t,t') = [\Sigma^r_\xi(t',t)]^*$. Furthermore, $f_\xi(\epsilon) = [e^{(\epsilon-\mu_\xi)/k_BT}+1]^{-1}$ is the Fermi-Dirac distribution of the electrons in the lead ξ, with k_B the Boltzmann constant, T the temperature, while $\Gamma_\xi(\epsilon)$ is the tunnel coupling to the lead ξ. Using the self-energies defined above and applying the double Fourier transformations in Eq. (2), in the wide-band limit in which Γ_ξ is energy independent one obtains

$$I_{\xi\nu}(t) = 2q_\nu\Gamma_\xi \mathrm{Im}\int\frac{d\epsilon}{2\pi}\int\frac{d\epsilon'}{2\pi}e^{-i(\epsilon-\epsilon')t} \times \sum_{m,n} J_m\left(\frac{v^\xi_{ac}}{\Omega}\right)J_n\left(\frac{v^\xi_{ac}}{\Omega}\right)e^{i(m-n)\phi_\xi} \times \mathrm{Tr}\big\{\hat{\sigma}_\nu[f_\xi(\epsilon'_m)\hat{G}^r(\epsilon,\epsilon'_{mn}) + \frac{1}{2}\hat{G}^<(\epsilon,\epsilon'_{mn})]\big\}, \qquad (3)$$

where we used the abbreviations $\epsilon_m = \epsilon - m\Omega$ and $\epsilon_{mn} = \epsilon - (m-n)\Omega$. The generating function $\exp[ia\sin(\Omega t + \phi)] = \sum_m J_m(a)\exp[im(\Omega t+\phi)]$ was used in Eq. (3), where J_m is the Bessel function of the first kind of order m.

The matrix components of the retarded Green's function of the electrons in the molecular orbital, in the absence of the ac harmonic potentials in the leads, can be obtained exactly by applying Dyson's expansion and analytic continuation rules.[16] Their double Fourier transforms are written as[59]

$$\mathcal{G}^r_{\sigma\sigma}(\epsilon,\epsilon') = \frac{2\pi\delta(\epsilon-\epsilon')G^{0r}_{\sigma\sigma}(\epsilon)}{1-\gamma^2 G^{0r}_{\sigma\sigma}(\epsilon)G^{0r}_{-\sigma-\sigma}(\epsilon_\sigma)},$$
$$\mathcal{G}^r_{\sigma-\sigma}(\epsilon,\epsilon') = \frac{2\pi\gamma\delta(\epsilon_\sigma-\epsilon')G^{0r}_{\sigma\sigma}(\epsilon)G^{0r}_{-\sigma-\sigma}(\epsilon_\sigma)}{1-\gamma^2 G^{0r}_{\sigma\sigma}(\epsilon)G^{0r}_{-\sigma-\sigma}(\epsilon_\sigma)},$$

with $\gamma = JS\sin(\theta)/2$ and $\epsilon_\sigma = \epsilon - \sigma\omega_L$. The matrix elements of the corresponding lesser Green's function are obtained using the Fourier transfomed Keldysh equation $\hat{\mathcal{G}}^<(\epsilon,\epsilon') = \int d\epsilon''\hat{\mathcal{G}}^r(\epsilon,\epsilon'')\hat{\Sigma}^<_0(\epsilon'')\hat{\mathcal{G}}^a(\epsilon'',\epsilon')/2\pi$.[16] Here $\hat{\mathcal{G}}^a(\epsilon,\epsilon') = [\hat{\mathcal{G}}^r(\epsilon',\epsilon)]^\dagger$, and $\Sigma^<_0(\epsilon) = i\sum_\xi\Gamma_\xi f_\xi(\epsilon)$ is the lesser self-energy originating from the orbital-lead coupling in the absence of harmonic potentials in the leads. The retarded Green's functions $\hat{G}^{0r}$ of the electrons in the molecular orbital, in the presence of the static component of the molecular spin and the constant magnetic field $\vec{B}$, are found using the equation of motion technique,[60] and Fourier transformed read $\hat{G}^{0r}(\epsilon) = [\epsilon - \epsilon_0 - \Sigma^r_0(\epsilon) - \hat{\sigma}_z(g\mu_B B + JS_z)/2]^{-1}$,[54,59] where $\Sigma^r_0(\epsilon) = -i\Gamma/2$.

For a weak ac field $v^\xi_{ac} \ll \Omega$, the retarded and lesser Green's functions of the electrons in the molecular orbital can be obtained by applying Dyson's expansion, analytic continuation rules and the Keldysh equation.[16] Keeping only terms linear in v^ξ_{ac}/Ω they read

$$\hat{G}^r(\epsilon,\epsilon') \approx \hat{\mathcal{G}}^r(\epsilon,\epsilon') \qquad (4)$$

$$\hat{G}^<(\epsilon,\epsilon') \approx \hat{\mathcal{G}}^<(\epsilon,\epsilon') + i\sum_{\xi,n=\pm1} n\Gamma_\xi\frac{v^\xi_{ac}}{\Omega}e^{in\phi_\xi} \times \int\frac{d\epsilon''}{4\pi}[f_\xi(\epsilon''_n) - f_\xi(\epsilon'')]\hat{\mathcal{G}}^r(\epsilon,\epsilon''_n)\hat{\mathcal{G}}^a(\epsilon'',\epsilon')\,. \qquad (5)$$

In the rest of the paper we will stay in this limit.

The particle current contains the following contributions

$$I_{\xi\nu}(t) = I^{\omega_L}_{\xi\nu}(t) + I^\Omega_{\xi\nu}(t)\,. \qquad (6)$$

The first component represents the transport in the absence of ac-voltages in the leads. It has a static and a time-dependent contribution, which are both created by the precession of the molecular spin. This precession-induced current read

$$I^{\omega_L}_{\xi\nu}(t) = 2q_\nu\Gamma_\xi\mathrm{Im}\Big\{\int\frac{d\epsilon}{2\pi}\int\frac{d\epsilon'}{2\pi}e^{-i(\epsilon-\epsilon')t} \times \mathrm{Tr}\{\hat{\sigma}_\nu[\frac{1}{2}\hat{\mathcal{G}}^<(\epsilon,\epsilon') + f_\xi(\epsilon')\hat{\mathcal{G}}^r(\epsilon,\epsilon')]\}\Big\}. \qquad (7)$$

In the limit $\gamma^2 \to 0$, Eq. (7) reduces to the result obtained previously.[56] The second term of Eq. (6) is induced when an ac voltage is applied to lead ξ and can be expressed in linear order with respect to v_{ac}^{ξ}/Ω using Eqs. (3), (4) and (5) as

$$I_{\xi\nu}^{\Omega}(t) = q_\nu \sum_{\zeta,n=\pm1} n\Gamma_\xi\Gamma_\zeta \frac{v_{ac}^{\zeta}}{\Omega} \mathrm{Re}\int \frac{d\epsilon}{2\pi}\int \frac{d\epsilon'}{2\pi} e^{-i(\epsilon-\epsilon')t+in\phi_\zeta} \Big\{ \int \frac{d\epsilon''}{4\pi} \{[f_\zeta(\epsilon_n'') - f_\zeta(\epsilon'')]\mathrm{Tr}[\hat{\sigma}_\nu \hat{\mathcal{G}}^r(\epsilon,\epsilon_n'')\hat{\mathcal{G}}^a(\epsilon'',\epsilon')]\} - \frac{i}{\Gamma_\zeta}\delta_{\xi\zeta}[f_\zeta(\epsilon_n') - f_\zeta(\epsilon')]\mathrm{Tr}[\hat{\sigma}_\nu \hat{\mathcal{G}}^r(\epsilon,\epsilon_n')]\Big\}. \quad (8)$$

These expressions for the currents constitute the main results of the article. They allow us to calculate the dynamic charge and spin conductance properties of our molecular contact. Note, that spin currents are more conveniently discussed in terms of the spin-transfer torque[44–47] exerted by the inelastic spin-currents onto the spin of the molecule, given by

$$\vec{T}(t) = \vec{T}^{\omega_L}(t) + \vec{T}^{\Omega}(t) = -[\vec{I}_L(t) + \vec{I}_R(t)]\,. \quad (9)$$

Hence, in the remainder of the article we will concentrate on the ac-charge conductance and the dc-spin-transfer torque.

IV. CHARGE TRANSPORT

A. Dynamic charge conductance

In general, applying an arbitrary ac-bias voltage $V(t)$ to the leads of a junction will induce a time-dependent current $I(t)$. The dynamic conductance $G(t,t')$ is defined as the linear response of the current to the applied ac field

$$I(t) = \int dt' G(t,t')V(t'). \quad (10)$$

The time-dependent particle charge current is induced by the ac harmonic potentials in the leads, and hence may be given by

$$I_{\xi 0}^{\Omega}(t) = \int dt' \sum_\zeta G_{\xi\zeta}^c(t,t')V_{ac}^{\zeta}(t'). \quad (11)$$

This expression defines the conductance $G_{\xi\zeta}^c$ as the response of the particle charge current in lead ξ to the external ac perturbation in lead ζ. According to Eq. (8) the current in Eq. (11) is harmonic. Consequently, the dynamic charge conductance between leads ξ and ζ only depends on the time difference $G_{\xi\zeta}^c(t,t') = G_{\xi\zeta}^c(t-t')$. Hence, the particle charge current in terms of the Fourier transforms $G_{\xi\zeta}^c(\Omega)$ can be written as

$$I_{\xi 0}^{\Omega}(t) = \mathrm{Re}\Big\{\sum_\zeta G_{\xi\zeta}^c(\Omega)v_{ac}^{\zeta}e^{-i(\Omega t+\phi_\zeta)}\Big\}. \quad (12)$$

Combining equations (8) and (12), and taking into account that $G_{\sigma\sigma}^{0r}(\epsilon) - G_{\sigma\sigma}^{0a}(\epsilon-\Omega) = -(\Omega+i\Gamma)G_{\sigma\sigma}^{0r}(\epsilon)G_{\sigma\sigma}^{0a}(\epsilon-\Omega)$, the complex components $G_{\xi\zeta}^c(\Omega)$ can be obtained as

$$G_{\xi\zeta}^c(\Omega) = -\frac{e^2}{h}[\Gamma_\xi\Gamma_\zeta - \Gamma_\xi\delta_{\xi\zeta}(\Gamma - i\Omega)]\int d\epsilon \frac{[f_\zeta(\epsilon-\Omega) - f_\zeta(\epsilon)]}{\Omega}T^c(\epsilon,\Omega), \quad (13)$$

with the energy-dependent complex function $T^c(\epsilon,\Omega)$, which can be written as

$$T^c(\epsilon,\Omega) = \sum_{\sigma=\pm1} \frac{G_{\sigma\sigma}^{0r}(\epsilon)G_{\sigma\sigma}^{0a}(\epsilon-\Omega)[1+\gamma^2 G_{-\sigma-\sigma}^{0r}(\epsilon_\sigma)G_{-\sigma-\sigma}^{0a}(\epsilon_\sigma-\Omega)]}{[1-\gamma^2 G_{\sigma\sigma}^{0a}(\epsilon-\Omega)G_{-\sigma-\sigma}^{0a}(\epsilon_\sigma-\Omega)][1-\gamma^2 G_{\sigma\sigma}^{0r}(\epsilon)G_{-\sigma-\sigma}^{0r}(\epsilon_\sigma)]}\,. \quad (14)$$

In order to determine the dynamic conductance under ac bias-voltage conditions, besides the particle current one needs to take into account the contribution from the displacement current. Coulomb interaction leads to screening of the charge accumulation in the quantum dot given by $I^d(t) = \frac{dQ(t)}{dt} = -e\mathrm{Im}\{\frac{d}{dt}[\mathrm{Tr}\hat{G}^<(t,t)]\}$. According to the Kirchoff's law $I^d(t) + \sum_\xi I_{\xi 0}^{\Omega}(t) = 0$. The following expression defines the total conductance of charge current $G_{\xi\zeta}$

$$I_{\xi 0}^{\Omega,tot}(t) = \mathrm{Re}\Big\{\sum_\zeta G_{\xi\zeta}(\Omega)v_{ac}^{\zeta}e^{-i(\Omega t+\phi_\zeta)}\Big\}, \quad (15)$$

while the displacement conductance G_ζ^d is given by

$$I^d(t) = \mathrm{Re}\Big\{\sum_\zeta G_\zeta^d(\Omega)v_{ac}^{\zeta}e^{-i(\Omega t+\phi_\zeta)}\Big\}. \quad (16)$$

The conservation of the total current and gauge invariance with respect to the shift of the chemical potentials lead to $\sum_\xi G_{\xi\zeta} = 0$ and $\sum_\zeta G_{\xi\zeta} = 0$.[40] These equations are satisfied by partitioning the displacement current into each lead[43] $I^{\Omega,tot}_{\xi 0} = I^{\Omega}_{\xi 0} + A_\xi I^d$, or equivalently $G_{\xi\zeta} = G^c_{\xi\zeta} + A_\xi G^d_\zeta$ in such a way that the sum of the partitioning factors A_ξ obeys $\sum_\xi A_\xi = 1$. Using the sum rules given above one obtains the expression for the dynamic conductance[40,43]

$$G_{\xi\zeta} = G^c_{\xi\zeta} - G^d_\zeta \frac{\sum_\lambda G^c_{\xi\lambda}}{\sum_\lambda G^d_\lambda}, \tag{17}$$

where $A_\xi = -(\sum_\lambda G^c_{\xi\lambda})/(\sum_\lambda G^d_\lambda)$, and $G^d_\zeta = -\sum_\xi G^c_{\xi\zeta}$, $G(\Omega) = G_{LL}(\Omega) = G_{RR}(\Omega) = -G_{LR}(\Omega) = -G_{RL}(\Omega)$. The first term of Eq. (17) represents the dynamic response of the charge current, while the second term is the internal response to the applied external ac perturbation due to screening by Coulomb interaction. Note that the dynamic conductance consists of a real dissipative component G_R and an imaginary nondissipative component G_I indicating the difference in phase between the current and the voltage. Due to the total current conservation the two terms in Eq. (17) should behave in a way that a minimum (maximum) of $G^c_{\xi\zeta}(\Omega)$ corresponds to a maximum (minimum) of $G^d_\zeta(\Omega)$, for both real and imaginary parts.

B. Density of states in molecular orbital

We now analyze the charge conductance in response to the ac-voltages. Since the dynamic conductance is an experimentally directly accessible quantity, we hope that a measurement can help to reveal the internal time scales of the coupling between the molecular and electronic spins in the transport. We begin by analyzing the density of states available for electron transport in the quantum dot

$$\rho(\epsilon) = -\frac{1}{\pi}\sum_{\sigma=\pm 1} \mathrm{Im}\left\{\frac{G^{0r}_{\sigma\sigma}(\epsilon)}{1-\gamma^2 G^{0r}_{\sigma\sigma}(\epsilon) G^{0r}_{-\sigma-\sigma}(\epsilon_\sigma)}\right\}. \tag{18}$$

The dc-bias transmission coefficient $T_{dc}(\epsilon) = 2\pi\Gamma_L\Gamma_R\rho(\epsilon)/\Gamma$ is plotted in Fig. 2(a) (black line). There are four resonant transmission channels. They manifest themselves as peaks positioned at (quasi-)energy levels $\epsilon_1 = \epsilon_\downarrow = \epsilon_0 - (\omega_L + JS)/2$ (spin down), $\epsilon_2 = \epsilon_\downarrow + \omega_L = \epsilon_0 + (\omega_L - JS)/2$ (spin up), $\epsilon_3 = \epsilon_\uparrow - \omega_L = \epsilon_0 - (\omega_L - JS)/2$ (spin down) and $\epsilon_4 = \epsilon_\uparrow = \epsilon_0 + (\omega_L + JS)/2$ (spin up). According to the expression for $\rho(\epsilon)$ these resonances are given by the real part of the poles of $[1-\gamma^2 G^{0r}_{\sigma\sigma}(\epsilon) G^{0r}_{-\sigma-\sigma}(\epsilon_\sigma)]^{-1}$. The physical origin of this level configuration can be understood as follows. The electron spin is subject to two magnetic fields of the constant strength, external field $\vec{B}$ and the field $\frac{J\vec{S}(t)}{g\mu_B}$ produced by the molecular magnet. These two fields cause the splitting of the initial level ϵ_0 into levels $\epsilon_\downarrow$ and $\epsilon_\uparrow$. The time-dependent precessing component of the molecular spin creates additional states available for electron transport. Namely, due to the periodic motion of the molecular spin an electron can absorb or emit an energy ω_L accompanied with a spin-flip.[56] The two additional states are thus created at energies $\epsilon_\downarrow + \omega_L$ and $\epsilon_\uparrow - \omega_L$. Spin-flip processes due to rotating magnetic field were analyzed in Ref. 59. A similar mechanism was discussed in a recent work for a nanomechanical spin-valve in which inelastic spin-flip processes are assisted by molecular vibrations.[61]

The part of $\hat{H}_{\rm MO}(t)$ representing the interaction of the electron spin $\hat{\vec{s}}$ with the effective magnetic field $\vec{B}_{\rm eff}(t) = \vec{B} + \frac{J}{g\mu_B}\vec{S}(t)$ is given by $\hat{H}_{eff}(t) = g\mu_B \hat{\vec{s}}\vec{B}_{\rm eff}(t)$. This Hamiltonian can be transformed to the rotating reference frame attached to the end point of the molecular spin $\vec{S}(t)$, using unitary transformation $\hat{U}(t) = \exp(i\frac{\omega_L}{2}t\hat{\sigma}_z)$ as $\hat{\tilde{H}} = \hat{U}\hat{H}_{eff}\hat{U}^\dagger - i\hat{U}\dot{\hat{U}}^\dagger$. One obtains

$$\hat{\tilde{H}} = \frac{JS}{2}[\sin(\theta)\hat{\sigma}_x + \cos(\theta)\hat{\sigma}_z], \tag{19}$$

with its eigen spectrum $E_\pm = \pm\frac{JS}{2}$. According to Eq. (19), electron spin $\langle\hat{\vec{s}}\rangle$ will precess in the rotating frame around the effective magnetic field, given by the vector $\frac{JS}{g\mu_B}(\sin(\theta), 0, \cos(\theta))$, with the Rabi frequency $\widetilde{\omega} = JS$.[62,63] Quantum mechanically, the precessing component of the molecular spin allows transitions between spin-up and spin-down electron states. If an electron is initially, at time $t = 0$, in the spin-up state with energy $JS_z/2$ in the rotating frame, the probability of its spin-flip at an arbitrary time t is given by Rabi's formula[62,63]

$$\wp_{\uparrow\to\downarrow}(t) = \frac{S^2_\perp}{S^2}\sin^2\left(\frac{JS}{2}t\right). \tag{20}$$

For $S_\perp \ll S_z$, the probability of transition $\wp_{\uparrow\to\downarrow}(t) \to 0$. In the opposite case, for $S_z \ll S_\perp$, the probability $\wp_{\uparrow\to\downarrow}(t) \to 1$ for $t = (2n+1)\pi/JS$.

C. Analysis of dynamic conductance

Assuming equal chemical potentials of the leads $\mu_L = \mu_R = \mu$, we analyze the dynamic conductance $G(\Omega)$ at zero temperature. Since we work in the wide band limit, this symmetry simplifies the partitioning factors to $A_\xi = \Gamma_\xi/\Gamma$. Hence, Eq. (17) can be transformed into

$$G_{\xi\zeta}(\Omega) = \frac{e^2}{h}\int d\epsilon T_{\xi\zeta}(\epsilon,\Omega)\frac{f_\zeta(\epsilon-\Omega) - f_\zeta(\epsilon)}{\Omega}. \tag{21}$$

Here $T_{\xi\zeta}(\epsilon,\Omega)$ is the effective transmission function that can be expressed as $T(\epsilon,\Omega) = T_{LL}(\epsilon,\Omega) = T_{RR}(\epsilon,\Omega) = -T_{LR}(\epsilon,\Omega) = -T_{RL}(\epsilon,\Omega)$, which reads

$$T(\epsilon,\Omega) = \frac{\Gamma_L\Gamma_R}{\Gamma}(\Gamma - i\Omega)T^c(\epsilon,\Omega). \tag{22}$$

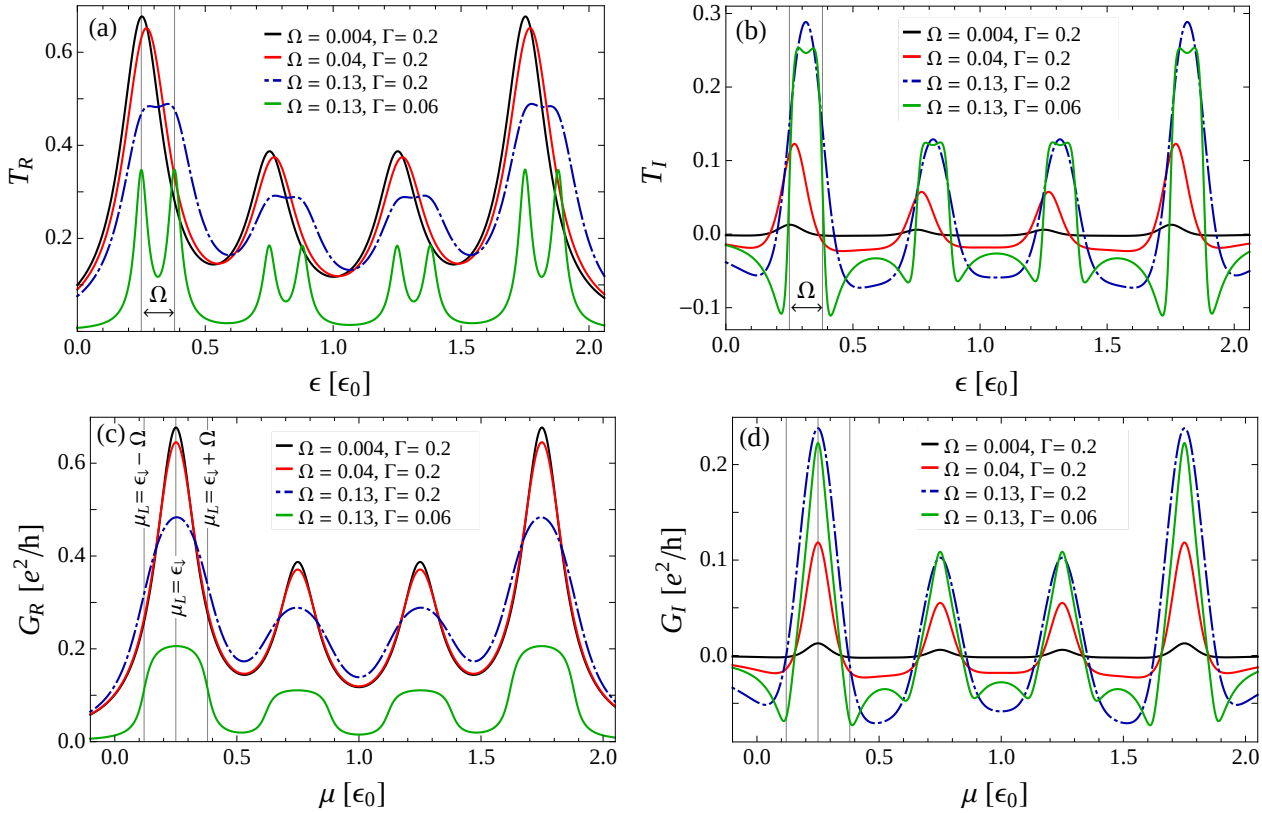

FIG. 2: (Color online) (a) Energy dependence of the real part T_R and (b) imaginary part T_I of the effective transmission function. (c) Real part G_R and (d) imaginary part G_I of the dynamic conductance as functions of the chemical potential μ, with $\mu = \mu_L = \mu_R$. All energies are given in the units of ϵ_0. Plots are obtained for different ac frequencies Ω and tunneling rates Γ at zero temperature, with $\vec{B} = B\vec{e}_z$, $\Gamma_L = \Gamma_R = \Gamma/2$. Other parameters are set to $\omega_L = 0.5\,\epsilon_0$, $J = 0.01\,\epsilon_0$, $S = 100$, $\theta = 1.25$, $\gamma \approx 0.474\,\epsilon_0$, $\epsilon_\uparrow = 1.75\,\epsilon_0$, and $\epsilon_\downarrow = 0.25\,\epsilon_0$.

In Figs. 2(a) and 2(b) we plotted the energy dependence of the real part $T_R(\epsilon, \Omega)$ and the imaginary part $T_I(\epsilon, \Omega)$ of the effective transmission function $T(\epsilon, \Omega)$, for several ac frequences Ω, at zero temperature. In the limit $\Omega \to 0$ (black lines in Fig. 2), $T_R(\epsilon, \Omega \to 0)$ coincides with the dc transmission function $T_{dc}(\epsilon)$, while $T_I(\epsilon, \Omega) \to 0$. Upon turning on the ac-bias voltage, due to the inelastic transport channels T_R decreases near each of the four resonances with increasing Ω, and splits into two different peaks distanced by Ω. Namely, the peaks positioned at ϵ_i and $\epsilon_i + \Omega$ appear as a signature of photon-assisted tunneling. They represent bands through which an electron can tunnel after it absorbs an energy Ω from the ac field. The photon-assisted bands through which the transport occurs are represented by the peaks on green (small Γ) and blue dot-dashed (larger Γ) lines in Fig. 2(a). Compared to Fig. 2(a), in Fig. 2(b) the peaks of T_I increase with increasing Ω.

The corresponding real part G_R and imaginary part G_I of the dynamic conductance versus chemical potential μ are plotted in Figs. 2(c) and 2(d). Both G_R and G_I achieve their maximum at $\mu_\xi = \epsilon_i$, where the resonance peaks are positioned. In accordance with Eq. (21) the electrons with energies $\mu_\zeta - \Omega \le \epsilon \le \mu_\zeta$ can participate in the transport processes by absorbing a photon of energy Ω. For $\Omega \to 0$ the dynamic conductance reaches its maximum near resonances and reduces to dc conductance $G_{\xi\zeta}(\Omega \to 0) = e^2 T_{\xi\zeta}(\mu_\zeta, \Omega \to 0)/h$. The dc conductance has four peaks emerging from the peaks in the resonant tunneling transmission function $T_{dc}(\epsilon)$ [black lines in Figs. 2(a) and 2(c)]. Following the behavior of T_I, the imaginary part of the dynamic conductance G_I approaches zero for $\Omega \to 0$ [black lines in Figs. 2(b) and 2(d)]. The considerable contribution of the displacement current to the total current is reflected in the decrease of G_R, and the increase of G_I near resonances with increasing Ω, as the displacement current opposes the change of the particle charge current under ac bias [red and blue dot-dashed lines in Figs. 2(c) and 2(d)]. For a small value of both Γ and Ω, complex components T_R and G_R show sharp resonant peaks. However, with the increase of Ω, each of the peaks in G_R broadens [green line in Fig. 2(c)]. It approaches a constant value around the corresponding resonant level, with the width equal to 2Ω, since the inequality

$$|\epsilon_i - \mu_\xi| \le \Omega \tag{23}$$

is the condition for the inelastic photon-assisted tunnel-

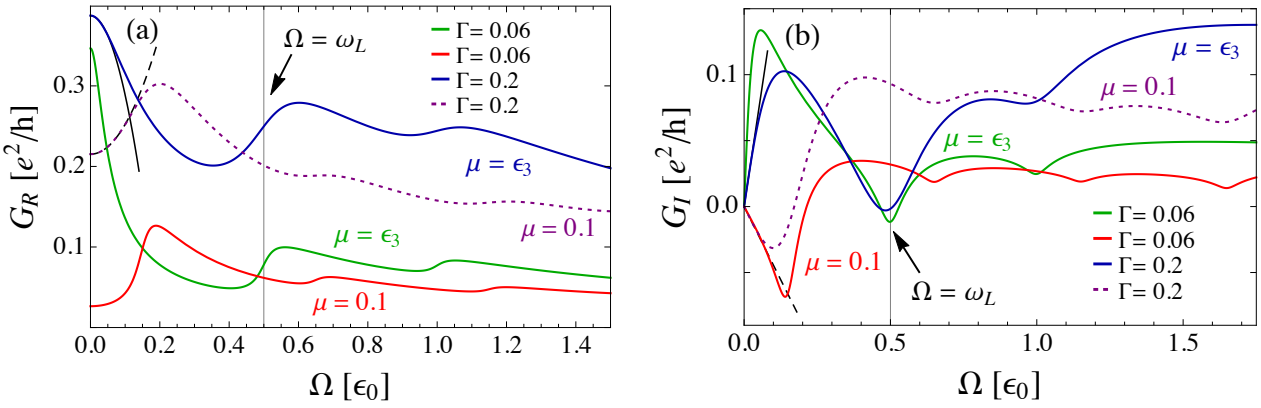

FIG. 3: (Color online) (a) Real part G_R and (b) imaginary part G_I of the dynamic conductance as functions of the ac frequency Ω. All energies are given in the units of ϵ_0. Plots are obtained for two different tunneling rates Γ and chemical potentials μ, with $\mu = \mu_L = \mu_R$, at zero temperature. Other parameters are set to $\Gamma_L = \Gamma_R = \Gamma/2$, $S = 100$, $J = 0.01\,\epsilon_0$, $\omega_L = 0.5\,\epsilon_0$, $\theta = 1.25$, $\gamma \approx 0.474\,\epsilon_0$, $\epsilon_\uparrow = 1.75\,\epsilon_0$, and $\epsilon_\downarrow = 0.25\,\epsilon_0$. In the resonant case $\mu = \epsilon_3 = \epsilon_\uparrow - \omega_L$, the response of the system is inductive-like in the low ac frequency limit ($G_I > 0$), and both G_R and G_I are enhanced for $\Omega = \omega_L$, as the channel with energy ϵ_4 becomes available for photon-assisted tunneling, i.e., $\mu + \Omega = \epsilon_4$.

ing to occur.

D. Frequency dependence of the ac conductance and equivalent circuit

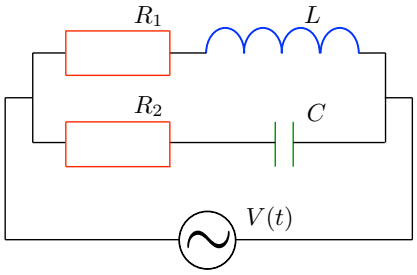

FIG. 4: (Color online) The equivalent classical circuit of the single-molecule magnet junction in the low ac frequency regime. It is composed of two serial combinations: one of a resistor and an inductor, and the other of a resistor and a capacitor, connected in parallel, and driven by a source of ac-voltage $V(t)$. The resistances are denoted by R_1 and R_2, L is the inductance, and C is the capacitance of the circuit elements.

In this subsection we analyze the behavior of the dynamic conductance components G_R and G_I as functions of the ac frequency Ω for $\mu = \epsilon_\uparrow - \omega_L = \epsilon_3$ [Fig. 3, green and blue lines] and $\mu = 0.1\,\epsilon_0$ [Fig. 3, red and purple-dotted lines] for two values of Γ at zero temperature.

The behavior of the ac-conductance components in the low ac-frequency regime can be understood using an effective circuit theory.[64] Namely, at small ac frequencies $\Omega \ll \Gamma$, the single-molecule magnet junction behaves as a parallel combination of two serial connections: one of a resistor and an inductor and the other of a resistor and a capacitor, i.e., as an RLC circuit [see Fig. 4]. Depending on the phase difference between the voltage and the current, the circuit shows inductive-like (positive phase difference) or capacitive-like (negative phase difference) responses to the applied ac voltage. Therefore, the dynamic conductance can be expanded up to the second order in Ω in the small ac-frequency limit in the following way:

$$G(\Omega) = G(0) + G'(0)\Omega + \frac{1}{2}G''(0)\Omega^2 + O(\Omega^3) \qquad (24)$$
$$\approx \frac{1}{R_1} + i\left(\frac{L}{R_1^2} - C\right)\Omega + \left(R_2C^2 - \frac{L^2}{R_1^3}\right)\Omega^2,$$

where R_1, R_2, L and C denote the resistances, inductance and capacitance of the circuit. In our further analysis we will assume that $R_1 = R_2 = R$. The first term of Eq. (24) represents therefore the dc conductance $G(0) = 1/R$. The second, imaginary term, linear in Ω is iG_I in the low frequency regime.

Depending on the sign of $L/R^2 - C$, the linear response is inductive-like ($G_I > 0$) while G_R decreases, or capacitive-like ($G_I < 0$) while G_R increases with the increase of Ω. For $C = L/R^2$ the system behaves like a resistor with $G = G(0)$. The nondissipative component G_I shows inductive-like behavior for

$$|\epsilon_i - \mu_\xi| < \frac{\Gamma}{2}, \qquad (25)$$

as we have observed in Fig. 2(d) (red line), and capacitive-like otherwise. The equality sign corresponds to resistive behavior.

The real part G_R is an even, while the imaginary part G_I is an odd function of Ω. In the low ac-frequency regime $\Omega \ll \Gamma$, G_R is a quadratic function [black, solid and dashed lines in Fig. 3 (a)], while G_I is a linear function of frequency [black, solid and dashed lines in Fig.

3(b)]. By fitting parameters of these functions and using Eq. (24), one obtains R, L, and C components, confirming that in this limit the ac conductance of the system resembles the previously described classical circuit model. The effective circuit parameters can be calculated in terms of the dynamic conductance according to Eq. (24). Note that they depend on the relative position of the Fermi energy of the leads with respect to the (quasi-)energy levels in the molecular orbital.

Near the four resonances we expect the system to be highly transmissive and therefore to conduct well. This is confirmed by Figs. 2 and 3. Namely, the imaginary conductance component $G_I > 0$ around resonances and is a positive linear function of Ω in the low frequency limit [see Fig. 3(b), black solid line]. This implies that the behavior of the system is inductive-like since the displacement current tends to reduce the charge current, as electrons reside awhile in the quantum dot, causing the delay in phase between the voltage and the current. Accordingly, the real component G_R decreases quadratically from initial value $G(0)$ upon switching on the ac frequency Ω [black solid line in Fig. 3(a)]. However, the off-resonance behavior is capacitive-like resulting from intra-orbital Coulomb interactions, which lead to the charge accumulation. Hence, in the low ac frequency limit $G_I(\Omega)$ is negative, and decreases linearly with the increase of Ω for Fermi surface energies of the leads which are far from the resonant energies ϵ_i [black dashed line in Fig. 3(b)]. In this case $G_R(\Omega)$ increases quadratically with Ω [black dashed line in Fig. 3(a)]. Obviously the single-molecule magnet junction behaves as an effective circuit only in the low frequency regime.

For higher ac-frequencies Ω we use Eq. (21) to analyze the behavior of G_R and G_I [see Fig. 3], where the dynamic response of the system remains predominantly inductivelike for $\mu = \epsilon_\uparrow - \omega_L = \epsilon_3$. With further increase of Ω, the ac conductance $G(\Omega)$ vanishes asymptotically. Upon turning on the ac frequency while the system is on resonance $\mu = \epsilon_\uparrow - \omega_L$, the imaginary component G_I increases quickly from 0 to a local maximum and then decreases to its minimum value for $\Omega = \omega_L$ [green and blue lines in Fig. 3(b)]. The real part G_R decreases to a local minimum and then has a step increase towards a local maximum around $\Omega = \omega_L$ [green and blue lines in Fig. 3(a)]. This behavior of the dynamic conductance can be understood as follows. For $\mu = \epsilon_\uparrow - \omega_L$, at $\Omega = \omega_L$, besides resonant level with energy $\epsilon_\uparrow - \omega_L$, the upper resonant level with energy $\epsilon_\uparrow$ becomes available for photon-assisted electron transport. It is then distanced by the energy Ω from the chemical potential μ. Consequently, an electron with Fermi energy equal to $\epsilon_\uparrow - \omega_L$ can absorb a photon of energy $\Omega = \omega_L$ and tunnel into the resonance level with energy $\epsilon_\uparrow$. This leads to an enhancement of the response functions G_R and G_I, with features corresponding to photon- assisted tunneling processes. Each step increase of G_R and the corresponding peak of G_I in Fig. 3 are determined by the difference between the (quasi-)energy levels ϵ_i and the chemical potential μ, viz. $|\epsilon_i - \mu| = \Omega$. Thus, for $\mu = \epsilon_3$ and the set of parameters given in Fig. 3, these steps and peaks are positioned around $\Omega/\epsilon_0 = 0.5$ and $\Omega/\epsilon_0 = 1$. For the larger tunnel couplings the steps in G_R are broadened due to the level broadening Γ. We notice that the enhancement of the dynamic conductance is higher for $\Omega = \omega_L$ than at the subsequent peak. This is due to the fact that the frequency has to traverse one resonant peak to reach the second one. We need to mention that the off-diagonal conductances $G_{\xi\zeta} = -G$, where $\xi \neq \zeta$, and hence have the opposite behavior than the diagonal ones.

In the spirit of the scattering matrix formalism the dynamic conductance of our single-molecule magnet junction, in the low ac-frequency regime, can be expanded as[65]

$$G_{\xi\zeta}(\Omega) = G_{\xi\zeta}(0) - i\Omega E_{\xi\zeta} + \Omega^2 K_{\xi\zeta} + O(\Omega^3), \qquad (26)$$

where $G_{\xi\zeta}(0)$ is the dc conductance. The quantity $E_{\xi\zeta} = -\mathrm{Im}\{\partial G_{\xi\zeta}(0)/\partial\Omega\}$ is called the emittance.[65] It contains the contribution from the displacement current and the partial density of states that characterize the scattering process.[41,66,67] The partial density of states can be calculated using the scattering matrix, and can be understood as density of states due to electrons injected from lead ζ and leaving through lead ξ.[41,66,67] The emittance $E_{\xi\zeta}$ measures the dynamic response of the system to an external oscillating ac field, and depending on its sign, the response is capacitive-like or inductive-like.[65] The matrix element of the third term, $K_{\xi\zeta} = \mathrm{Re}\{\partial^2 G_{\xi\zeta}(0)/\partial\Omega^2\}/2$, represents the correction to the real part of the dynamic conductance, and describes the dynamic dissipation in the low ac-frequency regime.[65] Both $E_{\xi\zeta}$ and $K_{\xi\zeta}$ obey the sum rules, since the total current conservation and gauge invariance conditions have to be satisfied.[40] According to Eq. (26), their diagonal elements $E = E_{\xi\xi}$ and $K = K_{\xi\xi}$ can be approximated as $E \approx -G_I/\Omega$ and $K \approx [G_R - G(0)]/\Omega^2$ in the low frequency limit.[65] Based on the analyzed G_R and G_I the behavior of E and K can be examined. Around all resonances $\mu = \epsilon_i$ the emittance $E < 0$ (inductive-like response), and $K < 0$ since $G_R < G(0)$, while off resonance $E > 0$ (capacitive-like response), and $K > 0$ [see Figs. 2(c), 2(d) and 3].

E. Effects of other parameters on the ac conductance

The conductance components G_R and G_I as functions of the Larmor precession frequency ω_L are presented in Figs. 5(a) and 5(b), while Figs. 5(c) and 5(d) depict the dependence of G_R and G_I on the exchange coupling constant J. They show similar characteristics as in Fig. 2, with higher peaks at resonancies corresponding to $\mu_\xi = \epsilon_{1,4}$, while lower peaks correspond to $\mu_\xi = \epsilon_{2,3}$. In the low ac frequency limit the system shows inductive-like behavior ($G_I > 0$) around resonancies for values of ω_L or J which satisfy the inequality (25) [see Figs. 5(c) and 5(d)]. The response of the system is resistive ($G_I = 0$) or

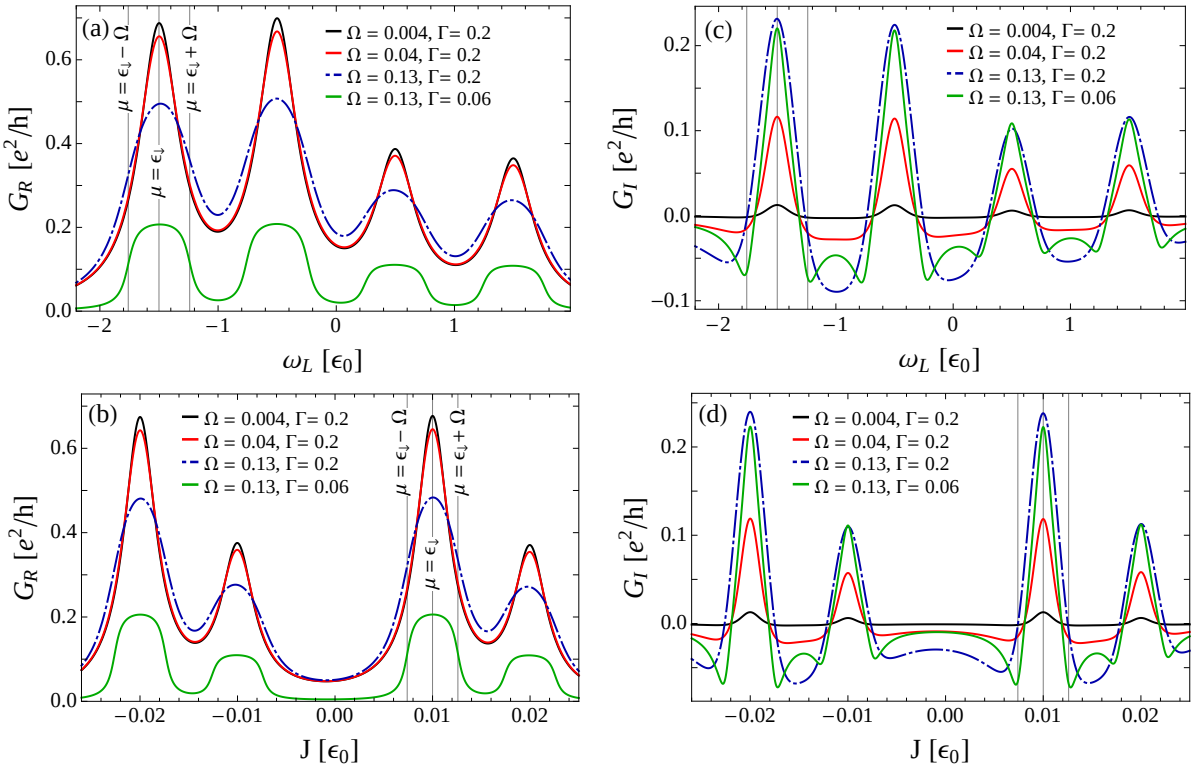

FIG. 5: (Color online) (a) Larmor frequency and (b) exchange coupling J dependence of the real part G_R of the dynamic conductance. (c) Larmor frequency and (d) exchange coupling J dependence of the imaginary part G_I of the dynamic conductance. In (a) and (c), $J = 0.01\,\epsilon_0$, and the chemical potentials of the leads are $\mu_L = \mu_R = 1.25\,\epsilon_0$, while in (b) and (d), the Larmor frequency is set to $\omega_L = 0.5\,\epsilon_0$, and the chemical potentials of the leads are $\mu_L = \mu_R = 0.25\,\epsilon_0$. All energies are given in the units of ϵ_0. Plots are obtained for different ac frequencies Ω and tunneling rates Γ at zero temperature, with $\vec{B} = B\vec{e}_z$, $\Gamma_L = \Gamma_R = \Gamma/2$. The molecular spin is set to $S = 100$, and the tilt angle to $\theta = 1.25$.

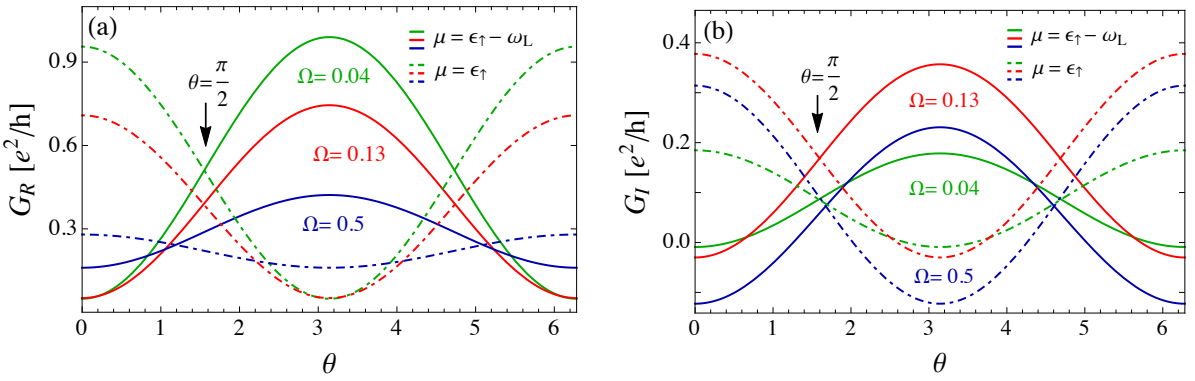

FIG. 6: (Color online) (a) Real part G_R and (b) imaginary part G_I of the dynamic conductance as functions of the tilt angle θ of the molecular spin $\vec{S}$ from the magnetic field $\vec{B} = B\vec{e}_z$. All energies are given in the units of ϵ_0. Plots are obtained for different values of Ω and μ, with $\mu = \mu_L = \mu_R$, at zero temperature. Other parameters are set to $S = 100$, $J = 0.01\,\epsilon_0$, $\omega_L = 0.5\,\epsilon_0$, $\Gamma = 0.2\,\epsilon_0$, and $\Gamma_L = \Gamma_R = \Gamma/2$. In the limit of low frequency Ω, for $\theta \to \pi/2$, the conductance component G_R, as well as G_I, approaches equal value at each resonance.

capacitive-like ($G_I < 0$) otherwise. In the limit of weak tunnel coupling Γ each peak of G_R broaden for large Ω approaching a constant value. Their width is equal to 4Ω and $4\Omega/S$ in Figs. 5(a) and 5(b) (green lines), since both ω_L and J fulfill the inequality (23) as the necessary condition for photon-assisted tunneling.

For $\theta = 1.25$ the peaks of both G_R and G_I in Figs. 2(c) and 2(d) at $\mu = \epsilon_{\uparrow,\downarrow} \mp \omega_L$ are much smaller than those at $\mu = \epsilon_{\uparrow,\downarrow}$, implying that the molecular magnet junction is less transmissive at the upper two mentioned res-

onances. This can be qualitatively understood by looking at Figs. 6(a) and 6(b) where we plotted G_R and G_I as functions of the angle θ between the molecular spin $\vec{S}$ and the external field $\vec{B}$. The behavior of the conductance components near the resonances for $\mu = \epsilon_\uparrow - \omega_L$ (solid lines in Fig. 6) and $\mu = \epsilon_\uparrow$ (dot-dashed lines in Fig. 6) depends on the direction of $\vec{S}$ with respect to the external magnetic field. For $\theta = 0$ the molecular spin $\vec{S}$ is static and the only two levels available for electron transport are Zeeman levels $\epsilon_1 = \epsilon_\downarrow$ and $\epsilon_4 = \epsilon_\uparrow$. In this case, when the system is at the resonance $\mu = \epsilon_\uparrow$, the components G_R and G_I take their maximum values, and $G_I > 0$ displaying an inductive-like behavior. For $\mu = \epsilon_\uparrow - \omega_L$ and $\theta = 0$, both G_R and G_I take their minimum values. There is no transmission channel at this energy for $\theta = 0$, but Γ is relatively large, and $G_I < 0$ displaying a capacitive-like response. With the increase of θ, the additional two channels at energies $\epsilon_\uparrow - \omega$ and $\epsilon_\downarrow + \omega_L$ appear, and become available for electron transport. This leads to the increase of conductance components G_R and G_I at $\mu = \epsilon_\uparrow - \omega_L$, and their decrease at $\mu_L = \epsilon_\uparrow$, as functions of θ (see Fig. 6). For $\theta \to \pi/2$, in the case of small Ω the complex components of the effective transmission function $T(\epsilon, \Omega)$ approach the same height at resonant energies ϵ_i, so that the probability of transmission reaches equal value at each level. Thus, the dynamic response function G_R approaches equal characteristics at each resonance as well as G_I. The points of intersection of solid and dot-dashed curves of the same color in Fig. 6 correspond to this particular case. For larger frequencies Ω, these points are shifted away from $\theta \to \pi/2$, since the peaks broaden and overlap and the suppression or increase of G_R and G_I is much faster. Finally, for $\theta = \pi$ the situation is reversed compared to the one with $\theta = 0$, as the again static spin $\vec{S}$ is in the opposite direction than that of the external field $\vec{B}$. The Zeeman splitting in this case is equal to $\omega_L - JS$, so that the only two levels available for electron transport are ϵ_2 and ϵ_3. Therefore, for $\theta = \pi$, when the system is at the resonance $\mu = \epsilon_3$, the conductance components G_R and G_I reach their maximum values, with $G_I > 0$. For $\mu = \epsilon_4$, which is off resonance for $\theta = \pi$, both G_R and G_I take minimum values, with $G_I < 0$.

V. SPIN TRANSPORT AND SPIN-TRANSFER TORQUE

A. Resonant spin transport

In the absence of ac harmonic potentials in the leads, resonant tunneling takes place. The spin-angular momenta between the electronic spins in the molecular orbital and the precessing molecular spin are exchanged via exchange interaction, governed by the coupling constant J. Further simplification of Eq. (7) gives time-independent z-component of the spin current, $I^{\omega_L}_{Lz}$, and the in-plane $j = x, y$ time-dependent spin-current components, from the left lead

$$I^{\omega_L}_{Lj}(t) = [I^j_L(\omega_L)e^{-i\omega_L t} + I^{j*}_L(\omega_L)e^{i\omega_L t}]. \qquad (27)$$

The complex time-independent functions $I^x_L(\omega_L)$ and $I^y_L(\omega_L)$, and the spin current $I^{\omega_L}_{Lz}$ can be expressed as

$$\begin{aligned}
I^x_L(\omega_L) =& -i\int \frac{d\epsilon}{4\pi}\Bigg\{\frac{\Gamma_L\Gamma_R}{\Gamma}[f_L(\epsilon)-f_R(\epsilon)]\Bigg[\frac{\gamma G^{0r}_{11}(\epsilon+\omega_L)G^{0r}_{22}(\epsilon)}{|1-\gamma^2 G^{0r}_{11}(\epsilon+\omega_L)G^{0r}_{22}(\epsilon)|^2} \qquad (28)\\
&+\frac{2i\gamma \mathrm{Im}\{G^{0r}_{11}(\epsilon)\}G^{0a}_{22}(\epsilon-\omega_L)+\gamma^3|G^{0r}_{11}(\epsilon)G^{0r}_{22}(\epsilon-\omega_L)|^2}{|1-\gamma^2 G^{0r}_{11}(\epsilon)G^{0r}_{22}(\epsilon-\omega_L)|^2}\Bigg]\\
&+\sum_{\xi,\zeta=L,R}\frac{\Gamma_\xi\Gamma_\zeta}{\Gamma}[f_\xi(\epsilon-\omega_L)-f_\zeta(\epsilon)]\Big[\delta_{\zeta L}-\delta_{\xi L}\gamma^2 G^{0a}_{11}(\epsilon)G^{0r}_{22}(\epsilon-\omega_L)\Big]\frac{\gamma G^{0r}_{11}(\epsilon)G^{0a}_{22}(\epsilon-\omega_L)}{|1-\gamma^2 G^{0r}_{11}(\epsilon)G^{0r}_{22}(\epsilon-\omega_L)|^2}\Bigg\},\\
I^y_L(\omega_L) =& \; iI^x_L(\omega_L), \qquad (29)\\
\text{and}\quad I^{\omega_L}_{Lz} =& \int\frac{d\epsilon}{4\pi}\Bigg\{\frac{\Gamma_L\Gamma_R}{\Gamma}[f_L(\epsilon)-f_R(\epsilon)]\Bigg[\frac{2\mathrm{Im}\{G^{0r}_{11}(\epsilon)\}}{|1-\gamma^2 G^{0r}_{11}(\epsilon)G^{0r}_{22}(\epsilon-\omega_L)|^2}-\frac{2\mathrm{Im}\{G^{0r}_{22}(\epsilon)\}}{|1-\gamma^2 G^{0r}_{11}(\epsilon+\omega_L)G^{0r}_{22}(\epsilon)|^2}\Bigg] \qquad (30)\\
&+\sum_{\xi,\zeta=L,R}\Gamma_\xi\Gamma_\zeta[f_\xi(\epsilon-\omega_L)-f_\zeta(\epsilon)](\delta_{\xi L}+\delta_{\zeta L})\frac{\gamma^2|G^{0r}_{11}(\epsilon)G^{0r}_{22}(\epsilon-\omega_L)|^2}{|1-\gamma^2 G^{0r}_{11}(\epsilon)G^{0r}_{22}(\epsilon-\omega_L)|^2}\Bigg\}.
\end{aligned}$$

The spin-transport properties are characterized by elastic, i.e., energy-conserving tunnel processes [first terms in Eqs. (28)-(30)], and inelastic, i.e., energy-nonconserving tunnel processes [terms involving factors $[f_\xi(\epsilon-\omega_L)-f_\zeta(\epsilon)]$ in Eqs. (28)-(30)]. In the later ones an electron changes its energy by ω_L and flips its spin due

to the exchange interaction with the rotational component of the molecular spin. The spin-flip processes occur between levels with energies $\epsilon_\uparrow$ and $\epsilon_\uparrow - \omega_L$, and between levels with energies $\epsilon_\downarrow$ and $\epsilon_\downarrow + \omega_L$.

The STT exerted by the inelastic spin-currents onto the spin of the molecule is given by[44–47]

$$\vec{T}^{\omega_L}(t) = -[\vec{I}_L^{\omega_L}(t) + \vec{I}_R^{\omega_L}(t)], \tag{31}$$

with its contribution to the molecular spin's dynamics as

$$\dot{\vec{S}}(t) = g\mu_B \vec{B} \times \vec{S}(t) + \vec{T}^{\omega_L}(t). \tag{32}$$

Using Eqs. (27)-(31), the STT can be expressed in terms of the matrix elements of the Green's functions $\hat{G}_0^r(\epsilon)$ and $\hat{G}_0^a(\epsilon)$ as

$$\begin{aligned} T_j^{\omega_L}(t) = &- \int \frac{d\epsilon}{2\pi} \sum_{\xi\zeta} \frac{\Gamma_\xi \Gamma_\zeta}{\Gamma} [f_\xi(\epsilon - \omega_L) - f_\zeta(\epsilon)] \\ &\times \mathrm{Im}\Big\{ (\hat{\sigma}_j)_{21} \frac{\gamma G_{11}^{0r}(\epsilon) G_{22}^{0a}(\epsilon - \omega_L)}{|1 - \gamma^2 G_{11}^{0r}(\epsilon) G_{22}^{0r}(\epsilon - \omega_L)|^2} \\ &\times [1 - \gamma^2 G_{11}^{0a}(\epsilon) G_{22}^{0r}(\epsilon - \omega_L)] e^{-i\omega_L t} \Big\}, \end{aligned} \tag{33}$$

$$\begin{aligned} T_z^{\omega_L} = &- \int \frac{d\epsilon}{2\pi} \sum_{\xi\zeta} \Gamma_\xi \Gamma_\zeta [f_\xi(\epsilon - \omega_L) - f_\zeta(\epsilon)] \\ &\times \frac{\gamma^2 |G_{11}^{0r}(\epsilon) G_{22}^{0r}(\epsilon - \omega_L)|^2}{|1 - \gamma^2 G_{11}^{0r}(\epsilon) G_{22}^{0r}(\epsilon - \omega_L)|^2}. \end{aligned} \tag{34}$$

Regarding the moecular spin $\vec{S}$ the STT can be presented as

$$\vec{T}^{\omega_L}(t) = \frac{\alpha}{S} \dot{\vec{S}}(t) \times \vec{S}(t) + \beta \dot{\vec{S}}(t) + \eta \vec{S}(t), \tag{35}$$

with the Gilbert damping coefficient α in the first term. The coefficient β that characterizes the modulation of the precession frequency of the molecular spin $\vec{S}$ is given by the second term. The third coefficient η can be written in terms of α and $T_z^{\omega_L}$ as $\eta = (T_z^{\omega_L} + \omega_L S \alpha \sin^2(\theta))/S_z$. Using Eqs. (33), (34) and comparing them with Eq. (35), one obtains exact expressions for the torque coefficients α and β as

$$\alpha = -\frac{1}{\omega_L S} \int \frac{d\epsilon}{2\pi} \sum_{\xi\zeta} \Gamma_\xi \Gamma_\zeta [f_\xi(\epsilon - \omega_L) - f_\zeta(\epsilon)] \frac{(JS_z/2\Gamma)\mathrm{Im}\{G_{11}^{0r}(\epsilon) G_{22}^{0a}(\epsilon - \omega_L)\} - \gamma^2 |G_{11}^{0r}(\epsilon) G_{22}^{0r}(\epsilon - \omega_L)|^2}{|1 - \gamma^2 G_{11}^{0r}(\epsilon) G_{22}^{0r}(\epsilon - \omega_L)|^2}, \tag{36}$$

$$\beta = -\frac{J}{\omega_L} \int \frac{d\epsilon}{4\pi} \sum_{\xi\zeta} \frac{\Gamma_\xi \Gamma_\zeta}{\Gamma} [f_\xi(\epsilon - \omega_L) - f_\zeta(\epsilon)] \frac{\mathrm{Re}\{G_{11}^{0r}(\epsilon) G_{22}^{0a}(\epsilon - \omega_L)\} - \gamma^2 |G_{11}^{0r}(\epsilon) G_{22}^{0r}(\epsilon - \omega_L)|^2}{|1 - \gamma^2 G_{11}^{0r}(\epsilon) G_{22}^{0r}(\epsilon - \omega_L)|^2}. \tag{37}$$

In the limit $\gamma^2 \to 0$, the expressions (28)-(37) are in agreement with Ref. 56. In the strong exchange coupling limit $J \gg \Gamma$ both Gilbert damping coefficient α and the torque coefficient β drop to zero.

B. Photon-assisted spin transport

The spin current components indicating photon-assisted inelastic spin transport can be obtained by further simplification of Eq. (8). The in-plane x and y spin-current components consist of oscillating terms involving both ac frequency Ω and Larmor frequency ω_L. Experimentally, by adjusting $\Omega = \pm\omega_L$, these currents may be measurable. In this case they have one dc component and one component oscillating with frequency 2Ω. The photon-assisted spin currents read

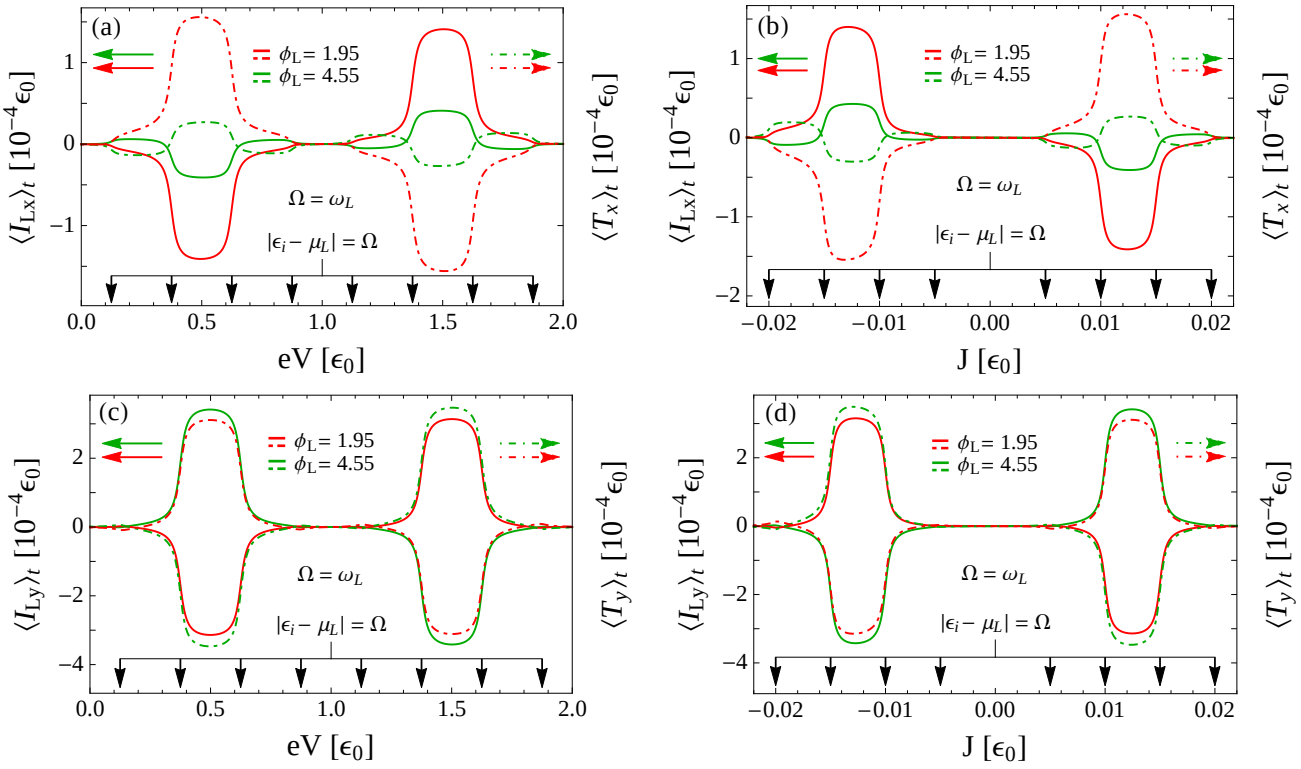

FIG. 7: (Color online) (a) Bias-voltage and (b) exchange coupling J dependence of the time-averaged spin-current and STT components $\langle I_{Lx}\rangle_t$ and $\langle T_x\rangle_t$. (c) Bias-voltage and (d) exchange coupling J dependence of the time-averaged spin-current and STT components $\langle I_{Ly}\rangle_t$ and $\langle T_y\rangle_t$. All energies are given in the units of ϵ_0. In (a) and (c), the exchange coupling constant is $J = 0.01\,\epsilon_0$, while in (b) and (d) the chemical potential of the left lead is set to $\mu_L = 0.375\,\epsilon_0$. Plots are obtained at zero temperature for two different phases ϕ_L, with $\vec{B} = B\vec{e}_z$. The other parameters are set to $\mu_R = 0$, $\phi_R = 0$, $v_{ac}^R = 0$, $v_{ac}^L = 0.02\,\epsilon_0$, $\theta = 1.25$, $S = 100$, $\Omega = \omega_L = 0.25\,\epsilon_0$, $\Gamma = 0.04\,\epsilon_0$, and $\Gamma_L = \Gamma_R = \Gamma/2$. Photon-assisted spin transport is enhanced for $\epsilon_1 < \mu_L < \epsilon_2$ and $\epsilon_1 < \mu_L < \epsilon_2$, where spin-current and STT in-plane components approach the constant largest magnitudes.

$$I^{\Omega}_{Lj}(t) = \sum_{\xi=L,R} \mathrm{Re}\Big\{[I^j_{L\xi}(\Omega)e^{-i(\Omega t+\phi_\xi)} + I^j_{L\xi}(-\Omega)e^{i(\Omega t+\phi_\xi)}]e^{-i\omega_L t}\Big\}, \qquad \text{for} \qquad j = x, y, \tag{38}$$

$$\text{where} \quad I^x_{L\xi}(\Omega) = \gamma\Gamma_L\Gamma_\xi \frac{v^\xi_{ac}}{\Omega}\int \frac{d\epsilon}{4\pi}[f_\xi(\epsilon-\Omega) - f_\xi(\epsilon)] \tag{39}$$

$$\times\Bigg\{\frac{G^{0a}_{11}(\epsilon-\Omega)G^{0a}_{22}(\epsilon-\Omega-\omega_L)\{G^{0r}_{11}(\epsilon) + i\frac{\delta_{L\xi}}{\Gamma_\xi}[1-\gamma^2 G^{0r}_{11}(\epsilon)G^{0r}_{22}(\epsilon-\omega_L)]\}}{[1-\gamma^2 G^{0r}_{11}(\epsilon)G^{0r}_{22}(\epsilon-\omega_L)][1-\gamma^2 G^{0a}_{11}(\epsilon-\Omega)G^{0a}_{22}(\epsilon-\Omega-\omega_L)]}$$

$$+\frac{G^{0r}_{11}(\epsilon+\omega_L)G^{0r}_{22}(\epsilon)\{G^{0a}_{22}(\epsilon-\Omega) - i\frac{\delta_{L\xi}}{\Gamma_\xi}[1-\gamma^2 G^{0a}_{11}(\epsilon-\Omega+\omega_L)G^{0a}_{22}(\epsilon-\Omega)]\}}{[1-\gamma^2 G^{0a}_{11}(\epsilon-\Omega+\omega_L)G^{0a}_{22}(\epsilon-\Omega)][1-\gamma^2 G^{0r}_{11}(\epsilon+\omega_L)G^{0r}_{22}(\epsilon)]}\Bigg\},$$

$$\text{while} \quad I^y_{L\xi}(\Omega) = iI^x_{L\xi}(\Omega), \tag{40}$$

$$\text{and} \quad I^{\Omega}_{Lz}(t) = \sum_{\xi=L,R}\sum_{\sigma=\pm1} \mathrm{Re}\Bigg\{\Gamma_L\Gamma_\xi\frac{v^\xi_{ac}}{\Omega}\int\frac{d\epsilon}{4\pi}[f_\xi(\epsilon-\Omega) - f_\xi(\epsilon)]e^{-i(\Omega t+\phi_\xi)} \tag{41}$$

$$\times\frac{[\hat{\sigma}_z\hat{G}^{0r}(\epsilon)\hat{G}^{0a}(\epsilon-\Omega)]_{\sigma\sigma}\Big\{2-[1-i\frac{\delta_{L\xi}}{\Gamma_\xi}(\Omega+i\Gamma)][1+\gamma^2 G^{0r}_{-\sigma-\sigma}(\epsilon_\sigma)G^{0a}_{-\sigma-\sigma}(\epsilon_\sigma-\Omega)]\Big\}}{[1-\gamma^2 G^{0r}_{\sigma\sigma}(\epsilon)G^{0r}_{-\sigma-\sigma}(\epsilon_\sigma)][1-\gamma^2 G^{0a}_{\sigma\sigma}(\epsilon-\Omega)G^{0a}_{-\sigma-\sigma}(\epsilon_\sigma-\Omega)]}\Bigg\}.$$

The time average of a periodic function $F(t)$, with the period T is defined as

$$\langle F\rangle_t = \frac{1}{T}\int_0^T F(t)dt. \tag{42}$$

According to Eq. (38), the time-averaged $j = x, y$ components of the total spin current $\vec{I}_L(t)$ are nonzero only

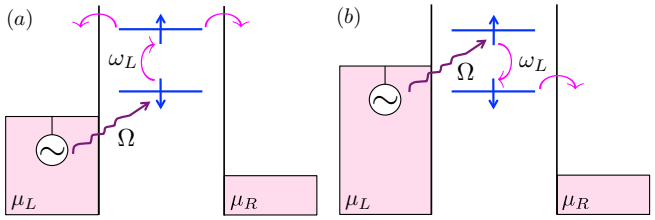

FIG. 8: (Color online) Sketch of two opposite photon-assisted spin-flip processes in the molecular orbital in the presence of ac harmonic potential with frequency Ω in the left lead. (a) Excited electron with energy Ω tunnels into spin-down level $\epsilon_\downarrow$ (or $\epsilon_\uparrow - \omega_L$). It absorbs an amount of energy ω_L, flips its spin due to the exchange interaction with the precessing component of the molecular spin, and exits the orbital. (b) Excited electron tunnels into spin-up level $\epsilon_\downarrow + \omega_L$ (or $\epsilon_\uparrow$), flips its spin and emits energy quantum ω_L. Then it tunnels out to the right lead.

for $\Omega = \pm\omega_L$ and read

$$\langle I_{Lj}\rangle_t = \langle I_{Lj}^{\Omega=\pm\omega_L}\rangle_t = \sum_\xi \mathrm{Re}\Big\{I_{L\xi}^j(\mp\Omega)e^{\pm i\phi_\xi}\Big\}, \quad (43)$$

while the time-averaged z spin-current component equals

$$\langle I_{Lz}\rangle_t = I_{Lz}^{\omega_L}. \quad (44)$$

The time-averaged STT is then given by

$$\langle \vec{T}\rangle_t = -\sum_\xi \langle \vec{I}_\xi\rangle_t. \quad (45)$$

Hence, the in-plane time-averaged x and y spin-current components contain only contributions from photon-assisted spin tunneling processes, while the z-component contains only contributions from resonant spin tunneling.

C. Analysis of the time-averaged spin transport

We start by analyzing the in-plane x and y components of the time-averaged spin current and STT, which differ in phase by $\pi/2$ according to Eqs. (40) and (43). They are presented as functions of the bias-voltage $eV = \mu_L - \mu_R$ in Figs. 7(a) and 7(c), and as functions of the exchange coupling constant J in Figs. 7(b) and 7(d). The plots are obtained at zero temperature, for two different phases of ac field in the left lead. We set $\Omega = \omega_L$, the right lead's Fermi energy $\mu_R = 0$, and apply an ac harmonic chemical potential only to the left lead. In Figs. 7(a) and 7(c) we vary the Fermi energy of the left lead as $\mu_L = eV$, while in Figs. 7(b) and 7(d) we set $\mu_L = 0.375\,\epsilon_0$. According to the segment $[f_L(\epsilon - \Omega) - f_L(\epsilon)]$ in Eq. (39), electrons with energies within the window $[\mu_L - \Omega, \mu_L]$ participate in the photon-assisted spin transport. Each of these processes is followed by a spin-flip and emission (apsorbtion) of an amount of energy ω_L. This is caused by the interaction of the electron spin with the precessing component of the molecular spin. In turn, during the exchange interaction a photon-assisted STT is generated onto $\vec{S}(t)$. In regard to resonant photon-assisted transmission of 1/2 - spin particles, the in-plane spin-current components show significant changes either in magnitude, or direction, controlled by the change of the phase of the ac field in the left lead ϕ_L. Similarly to the case of charge transport, the necessary condition for photon-assisted spin tunneling is given by the Eq. (23). The cases with equality sign in Eq. (23) are represented by the black arrows in Fig. 7, pointing to the eV scale. Each level satisfying this condition corresponds to two black arrows. In the region between each two black arrows the inequality (23) is satisfied for at least one (quasi-)energy level of the molecular orbital. Here spin currents and STT approach constant values. If $\epsilon_1 \le \mu_L \le \epsilon_2$ or $\epsilon_3 \le \mu_L \le \epsilon_4$, the Eq. (23) is satisfied for both ϵ_1 and ϵ_2, or ϵ_3 and ϵ_4. As a result, the magnitude of spin currents and STT is enhanced under these conditions, due to the involvement of both levels ϵ_1 and ϵ_2, or ϵ_3 and ϵ_4, in photon-assisted spin transport and photon-assisted spin-flip processes inside the molecular orbital. We should point out that both spin-current components and STTs are antisymmetric functions of eV with respect to the position of ϵ_0, and odd functions of exchange coupling J. This is a consequence of the antisymmetric position of levels ϵ_i attributed to spin-up or spin-down state of the electron with respect to ϵ_0. Using Eq. (43) and setting $\phi_R = 0$, we obtain the largest magnitudes of the $j = x, y$ time-averaged spin-currents for

$$\phi_L = \arctan\left(\frac{\mathrm{Im}\{I_{L\xi}^k(\mp\Omega)\}}{\mathrm{Re}\{I_{L\xi}^k(\mp\Omega)\}}\right), \quad (46)$$

where $\Omega = \pm\omega_L$. Simultaneously, the other in-plane time-averaged spin-current equals zero. The magnitude and direction of the time-averaged spin currents and STTs can also be controlled by changing the tilt angle θ. For $\theta = 0$, the in-plane spin currents are equal to 0. If μ_L lies between any two levels connected with spin-flip mechanism, then the largest magnitudes of the in-plane spin-current and STT components are obtained for $\theta = \pi/2$. In this case, the spin-flip is most probable, with the largest magnitude of the rotating field.

Some of the photon-assisted tunneling processes contributing to the spin transport are presented in Fig. 8. Here we show examples of two opposite photon-assisted spin-flip processes. Fig. 8(a) corresponds to the case in which $\epsilon_1 - \mu_L < \Omega$ (or $\epsilon_3 - \mu_L < \Omega$). Here an electron from the left lead excited by energy $\Omega = \omega_L$ tunnels into the level ϵ_1 (or ϵ_3). During the exchange interaction with the precessing component of $\vec{S}(t)$ it absorbs an energy ω_L and flips its spin, ending up in the level ϵ_2 (or ϵ_4), and then tunnels into either of the leads. One photon-assisted spin-flip process through level ϵ_2 (or ϵ_4) for $\epsilon_1 \le \mu_L \le \epsilon_2$ (or $\epsilon_3 \le \mu_L \le \epsilon_4$) is presented in Fig. 8(b). In this case an electron absorbs an energy $\Omega = \omega_L$ interacting with

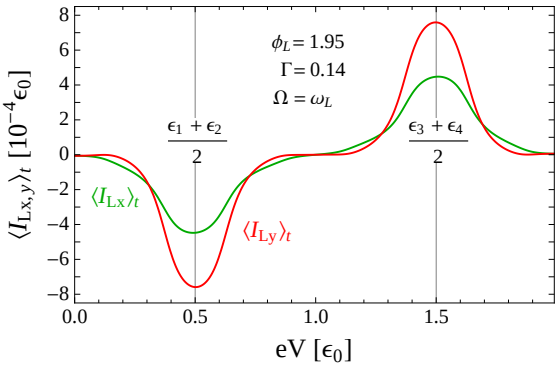

FIG. 9: (Color online) Time-averaged spin-current components $\langle I_{Lx} \rangle_t$ and $\langle I_{Ly} \rangle_t$ as functions of bias-voltage eV. The plots are obtained at zero temperature for $\Gamma = 0.14\,\epsilon_0$, with $\vec{B} = B\vec{e}_z$, $\Omega = \omega_L = 0.25\,\epsilon_0$, and $\Gamma_L = \Gamma_R = \Gamma/2$. All energies are given in the units of ϵ_0. The other parameters are set to $\mu_R = 0$, $v_{ac}^L = 0.02\,\epsilon_0$, $\phi_L = 1.95$, $v_{ac}^R = 0$, $\phi_R = 0$, $\theta = 1.25$, $J = 0.01\,\epsilon_0$ and $S = 100$. Grid lines correspond to peaks due to quantum interference effect between two opposite spin-states ϵ_1 (or ϵ_3) and ϵ_2 (or ϵ_4), distanced by ω_L in the molecular orbital.

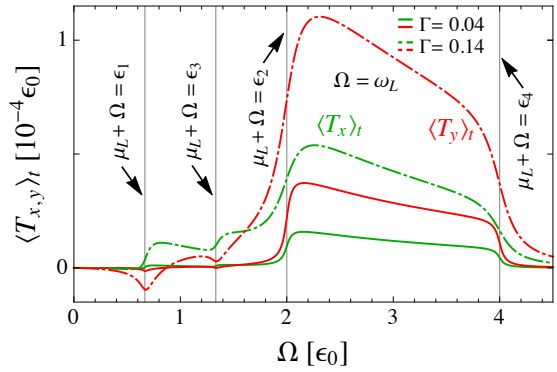

FIG. 10: (Color online) Time-averaged spin-transfer torque components $\langle T_x \rangle_t$ and $\langle T_y \rangle_t$ as functions of ac frequency Ω. The plots are obtained at zero temperature for two different Γ, with $\vec{B} = B\vec{e}_z$, $\Omega = \omega_L$, and $\Gamma_L = \Gamma_R = \Gamma/2$. All energies are given in the units of ϵ_0. The other parameters are set to $\mu_L = -0.5\,\epsilon_0$, $\mu_R = 0$, $v_{ac}^L = 0.02\,\epsilon_0$, $\phi_L = 1.95$, $v_{ac}^R = 0$, $\phi_R = 0$, $\theta = 1.25$, $J = 0.01\,\epsilon_0$ and $S = 100$. Each step or peak coincides with a change in the number of available channels for photon-assisted spin tunneling.

ac field in the left lead and enter the spin-up level ϵ_2 (or ϵ_4). Then it emits energy quantum ω_L and flips its spin due to the interaction with the precessing molecular spin, and tunnels off the molecular orbital into the right lead.

We analyzed the time-averaged photon-assisted spin transport for $\Gamma \ll \omega_L$. However, for Γ comparable with ω_L, we should take into account the possibility of quantum interference between spin states with energies ϵ_1 and ϵ_2, or ϵ_3 and ϵ_4. This effect is presented in Fig. 9, where it manifests itself in the form of two peaks located at $\mu_L = (\epsilon_1 + \epsilon_2)/2$ and $\mu_L = (\epsilon_3 + \epsilon_4)/2$.

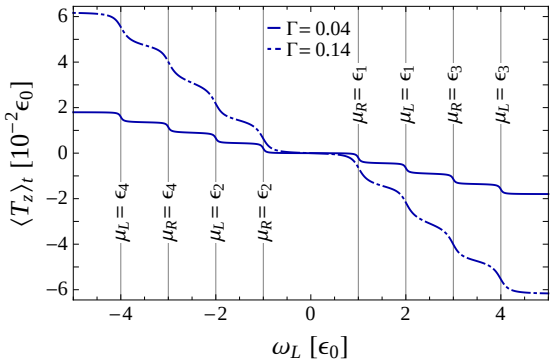

FIG. 11: (Color online) Time-averaged z component of the spin-transfer torque $\langle T_z \rangle_t$ as a function of the Larmor precession frequency ω_L. Plots are obtained for two different tunneling rates Γ at zero temperature, with $\vec{B} = B\vec{e}_z$ and $\Gamma_L = \Gamma_R = \Gamma/2$. All energies are given in the units of ϵ_0. The other parameters are set to $\mu_L = -0.5\,\epsilon_0$, $\mu_R = 0$, $\theta = 1.25$, $J = 0.01\,\epsilon_0$ and $S = 100$. Each step corresponds to a resonant spin-tunneling process involving a spin-flip in the molecular orbital.

In Fig. 10 the STT x and y time-averaged components are plotted as functions of ac frequancy $\Omega = \omega_L$ for two different tunnel coupling constants $\Gamma = 0.04$ (solid lines) and $\Gamma = 0.14$ (dot-dashed lines) at zero temperature. The grid lines correspond to $\epsilon_i - \mu_L = \Omega$. For Ω such that $\epsilon_1 - \mu_L = \Omega$ the level ϵ_1 of the molecular orbital participates in photon-assisted spin transport, followed by an electron spin-flip, and hence a finite STT. In this case $\langle T_x \rangle_t$ is initially enhanced while $\langle T_y \rangle_t$ has a minimum value [first grid line in Fig. 10]. As Ω increases the inequality (23) is satisfied for level ϵ_1 leading to a nonzero STT. With further increase of ac frequency Ω the photon-assisted spin transport begins to take place in the level ϵ_3 resulting in another enhancement of $\langle T_x \rangle_t$ and a local minimum of $\langle T_y \rangle_t$. For larger Ω the Eq. (23) is satisfied for both ϵ_1 and ϵ_3. Consequently, both $\langle T_x \rangle_t$, and $\langle T_y \rangle_t$ increase. Finally, as Ω increases further, level ϵ_2 also becomes available for photon-assisted spin tunneling, leading to the largest enhancement of both STT components. As Ω increases Eq. (23) is satisfied for levels ϵ_1, ϵ_2 and ϵ_3 and photon-assisted STT components are large and decreasing. After the level ϵ_4 becomes available for photon-assisted spin transport, both components $\langle T_x \rangle_t$ and $\langle T_y \rangle_t$ drop to zero. This is due to the previously mentioned antisymmetry. Namely, in this case the contributions of the photon-assisted STTs for $\epsilon_1 < \mu_L < \epsilon_2$ and $\epsilon_3 < \mu_L < \epsilon_4$ are equal in magnitude, but have opposite directions. Therefore, they cancel each other as μ_L satisfies both these inequalities simultaneously. Conditions of Eq. (23) are relaxed for larger Γ due to the broadening of the energy levels ϵ_i.

The z component of the time-averaged STT, $\langle T_z \rangle_t$ is plotted as a function of the Larmor frequency ω_L in Fig. 11. This component does not contain contributions from photon-assisted spin tunneling, but only from resonant

tunneling, followed by an electron spin-flip due to the interaction with the precessing component of the molecular spin $\vec{S}$. In turn an STT is exerted on the molecular spin. The STT component $\langle T_z \rangle_t$ is an odd function of ω_L since the change of the direction of $\vec{B}$ gives negative ω_L. Each step in Fig. 11 denotes a new available resonant spin-transport channel, and an additional spin-flip process, contributing to the STT, which takes place for $\mu_\xi = \epsilon_i$.

VI. CONCLUSIONS

In this paper we have theoretically studied photon-assisted spin and charge transport through a single-molecule magnet junction. The junction consists of single molecular orbital in the presence of a molecular spin precessing with Larmor frequency ω_L in a constant magnetic field. The orbital is connected to two metal leads subject to harmonically varying chemical potentials with frequency Ω, treated as a perturbation. We used the Keldysh nonequilibrium Green's functions method to derive charge and spin currents and the spin-transfer torque. We employed the displacement current partitioning scheme of Wang *et al.*,[43] to obtain gauge invariant expressions for the dynamic conductance of the charge current. The dynamic response of the system is controlled by photon-assisted transport. In the low ac frequency limit this junction behaves as an effective inductor or capacitor depending on the system parameters. For $\Omega = \omega_L$, when the chemical potential μ_ξ is in resonance with a level ϵ_i in the molecular orbital, the ac conductance is enhanced. The photon-assisted x and y spin-current components consist of a dc part and a part that oscillates with frequency 2Ω for $\Omega = \omega_L$. This opens a possibility to experimentally investigate photon-assisted spin-transfer torque exerted on the single-molecule magnet, which can be detected through the presence of nonzero time-averaged contributions. By manipulating the phases of the harmonic potentials in the leads with respect to the precession, the control of the direction and the magnitude of the time-averaged photon-assisted spin transport and spin-transfer torque is achievable. Finally, in this work we present the nonperturbative Gilbert damping and other STT coefficients with respect to the coupling γ, in the zero ac frequency limit. Remarkably the Gilbert damping vanishes in the strong coupling limit.

In the future it might be interesting to investigate further transport properties like the current or the torque noise as well as to find ways to manipulate the magnetic moment using e.g. ferromagnetic leads.

Acknowledgments

We would like to thank Gianluca Rastelli, Federica Haupt and Cecilia Holmqvist for useful discussions. We gratefully acknowledge the financial support from the Deutsche Forschungsgemeinschaft through the SFB 767 *Controlled Nanosystems* and the SPP 1285 *Semiconductor Spintronics* and an ERC Advanced Grant *UltraPhase* of Alfred Leitenstorfer.

[1] A. Aviram and M. Ratner, Chem. Phys. Lett. **29**, 277 (1974).
[2] A. Nitzan and M. Ratner, Science **300**, 1384 (2003).
[3] J. C. Cuevas, E. Scheer, *Molecular Electronics: An Introduction to Theory and Experiment*, Word Scientific, Singapore, 2010.
[4] J. Lehmann, S. Kohler, P. Hänggi, and A. Nitzan, J. Chem. Phys. **118**, 3283 (2003); S. Kohler, J. Lehmann, and P. Hänggi, Phys. Rep. **406**, 379 (2005).
[5] D. Dulić, S. J. van der Molen, T. Kudernac, H. T. Jonkman, J. J. D. de Jong, T. N. Bowden, J. van Esch, B. L. Feringa, and B. J. van Wees, Phys. Rev. Lett. **91**, 207402 (2003).
[6] S. van der Molen, J. Liao, T. Kudernac, J. Agustsson, L. Bernard, M. Calame, B. van Wees, B. Feringa, and C. Schönenberger, Nano Lett. **9**, 76 (2009).
[7] H. Song, Y. Kim, Y. H. Jang, H. Jeong, M. A. Reed, and T. Lee, Nature (London) **462**, 1039 (2009).
[8] Y. Kim, T. J. Hellmuth, D. Sysoiev, F. Pauly, T. Pietsch, J. Wolf, A. Erbe, T. Huhn, U. Groth, U. E. Steiner, and E. Scheer, Nano Lett. **12**(7), 3736 (2012).
[9] W. Wernsdorfer and R. Sessoli, Science **284**, 133 (1999).
[10] J. R. Friedman, M. P. Sarachik, J. Tejada, and R. Ziolo, Phys. Rev. Lett. **76**, 3830 (1996); L. Thomas, F. Lionti, R. Ballou, D. Gatteschi, R. Sessoli, and B. Barbara, Nature (London) **383**, 145-147 (1996); C. Sangregorio, T. Ohm, C. Paulsen, R. Sessoli, and D. Gatteschi, Phys. Rev. Lett. **78**, 4645 (1997); W. Wernsdorfer, M. Murugesu, and G. Christou, *ibid.* **96**, 057208 (2006).
[11] A. Ardavan, O. Rival, J. J. L. Morton, S. J. Blundell, A. M. Tyryshkin, G. A. Timco, and R. E. P. Winpenny, Phys. Rev. Lett. **98**, 057201 (2007); S. Carretta, P. Santini, G. Amoretti, T. Guidi, J. R. D. Copley, Y. Qiu, R. Caciuffo, G. A. Timco, and R. E. P. Winpenny, *ibid.* **98**, 167401 (2007); S. Bertaina, S. Gambarelli, T. Mitra, B. Tsukerblat, A. Muller, and B. Barbara, Nature (London) **453**, 203 (2008).
[12] A. Garg, EuroPhys. Lett. **22**, 205 (1993); W. Wernsdorfer, N. E. Chakov, and G. Christou, Phys. Rev. Lett. **95**, 037203 (2005).
[13] D. D. Awschalom, M. E. Flatte, and N. Samarth, *Spintronics* (Scientific American, New York, 2002), pp. 67-73.
[14] N. S. Wingreen, A.-P.Jauho, and Y. Meir, Phys. Rev. B **48**, 8487 (1993).
[15] A.-P.Jauho, N. S. Wingreen, and Y. Meir, Phys. Rev. B **50**, 5528 (1994).
[16] A.-P. Jauho and H. Haug, *Quantum Kinetics in Transport and Optics of Semiconductors* (Springer, Berlin, 1998).
[17] B. Dong, H. L. Cui, and X. L. Lei, Phys. Rev. B **69**, 205315 (2004).

[18] Y. Zhu, J. Maciejko, T. Ji, H. Guo, and J. Wang, Phys. Rev. B **71**, 075317 (2005).
[19] E. Runge and E. K. U. Gross, Phys. Rev. Lett **52**, 997 (1984).
[20] G. Stefanucci and C. O. Almbladh, Europhys. Lett **67**, 14 (2004).
[21] K. Burke, R. Car, and R. Gebauer Phys. Rev. Lett **94**, 146803 (2005).
[22] S. Kurth, G. Stefanucci, C. O. Almbladh, A. Rubio, and E. K. U. Gross, Phys. Rev. B **72**, 035308 (2005).
[23] E. Khosravi, S. Kurth, G. Stefanucci, and E. K. U. Gross, Appl. Phys. A **93**, 355 (2008).
[24] G. Q. Li, S. Welack, M. Schreiber, and U. Kleinekathöfer, Phys. Rev. B **77**, 075321 (2008).
[25] A. H. L. Dayem and R. J. Martin, Phys. Rev. Lett. **8**, 246 (1962).
[26] P. K. Tien and J. P. Gordon, Phys. Rev. **129**, 647 (1963).
[27] G. Platero and R. Aguado, Phys. Rep. **395**, 1 (2004).
[28] W. Zheng, Y. Wei, J. Wang and H. Guo, Phys. Rev. B **61**, 13121 (2000); J. Wu, B. Wang, J. Wang, and H. Guo, Phys. Rev. B **72**, 195324 (2005).
[29] A. Tikhonov, R. D. Coalson, and Y. Dahnovsky, J. Chem. Phys. **116**, 10909 (2002).
[30] U. Kleinekathöfer, G.-Q. Li, S. Welack, and M. Schreiber, Europhys. Lett. **75**, 139 (2006); G.-Q. Li, M. Schreiber, and U. Kleinekathöfer *ibid.* **79**, 27006 (2007).
[31] J. K. Viljas and J. C. Cuevas, Phys. Rev. B **75**, 075406 (2007); J. K. Viljas, F. Pauly, and J. C. Cuevas, *ibid* **76**, 033403 (2007); J. K. Viljas, F. Pauly, and J. C. Cuevas, *ibid* **77**, 155119 (2008).
[32] L.-Y. Hsu and H. Rabitz, Phys. Rev. Lett. **109**, 186801 (2012).
[33] B. D. Fainberg, Phys. Rev. B **88**, 245435 (2013).
[34] Chauvin, M. and vom Stein, P. and Pothier, H. and Joyez, P. and Huber, M. E. and Esteve, D. and Urbina, C., Phys. Rev. Lett. **97**, 067006 (2006).
[35] D. C. Guhr, D. Rettinger, J. Boneberg, A. Erbe, P. Leiderer, and E. Scheer, Phys. Rev. Lett. **99**, 086801 (2007).
[36] N. Ittah, G. Noy, I. Yutsis, and Y. Selzer, Nano Lett. **9**, 1615 (2009).
[37] G. Noy, A. Ophir, and Y. Selzer, Angew. Chem. Int. Ed. **49**, 5734 (2010).
[38] M. A. Mangold, M. Calame, M. Mayor, and A. W. Holleitner, J. Am. Chem. Soc. **133**, 12185 (2011).
[39] M. Bütiker, H. Thomas, and A. Prêtre, Phys. Lett. A **180**, 364 (1993).
[40] M. Büttiker, A. Prêtre, and H. Thomas, Phys. Rev. Lett. **70**, 4114 (1993).
[41] M. Bütiker, J. Phys. Cond. Mat. **5**, 9361 (1993).
[42] Y. Wei and J. Wang, Phys. Rev. B **79**, 195315 (2009).
[43] B. G. Wang, J. Wang, and H. Guo, Phys. Rev. Lett. **82**, 398 (1999).
[44] J.C. Slonczewski, J. Magn. Magn. Mater. **159**, L1 (1996).
[45] L. Berger, Phys. Rev. B **54**, 9353 (1996).
[46] Y. Tserkovnyak, A. Brataas, G. E. W. Bauer, and B. I. Halperin, Rev. Mod. Phys. **77**, 1375 (2005).
[47] D. C. Ralph and M. D. Stiles, J. Magn and Magn. Mater. **320**, 1190 (2008).
[48] J. C. Slonczewski, Phys. Rev. B **71**, 024411 (2005).
[49] C. Timm and F. Elste, Phys. Rev. B **73**, 235304 (2006); F. Elste and C. Timm, Phys. Rev. B **73**, 235305 (2006).
[50] M. Misiorny and J. Barnaś, Phys. Rev. B **75**, 134425 (2007).
[51] J. C. Sankey, Y-T. Cui, J. Z. Sun, J. C. Slonczweski, R. A. Buhrman, and D. C. Ralph, Nat. Phys. **4**, 67 (2008).
[52] J. Xiao, G. E. W. Bauer, and A. Brataas, Phys. Rev. B **77**, 224419 (2008).
[53] F. Delgado, J. J. Palacios, and J. Fernández-Rossier, Phys. Rev. Lett. **104**, 026601 (2010).
[54] N. Bode, L. Arrachea, G. S. Lozano, T. S. Nunner, and F. von Oppen, Phys. Rev. B **85**, 115440 (2012).
[55] R. Sessoli, D. Gatteschi, A. Caneschi, and M. A. Novak, Nature (London) **365**, 141 (1993).
[56] M. Filipović, C. Holmqvist, F. Haupt, and W. Belzig, Phys. Rev. B **87**, 045426 (2013); **88**, 119901(E) (2013).
[57] T. L. Gilbert, Phys. Rev. 100, 1243 (1955); T. Gilbert, IEEE Trans. Magn. **40**, 3443 (2004).
[58] C. Kittel, Phys. Rev. **73**, 155 (1948).
[59] B. Wang, J. Wang, and H. Guo, Phys. Rev. B **67**, 092408 (2003).
[60] H. Bruus and K. Flensberg, *Many-Body Quantum Theory in Condensed Matter Physics* (Oxford University Press, Oxford, UK, 2004).
[61] P. Stadler, W. Belzig, and G. Rastelli, Phys. Rev. Lett. **113**, 047201 (2014).
[62] A. Abragam, *The Principles of Nuclear Magnetism*, Clarendon Press, Oxford (1961).
[63] C. Cohen-Tannoudji, B. Diu, F. Laloë, *Quantum Mechanics*, Volume One, John Wiley & Sons, Toronto (1977).
[64] A. Prêtre, H. Thomas, and M. Büttiker Phys. Rev. B **54**, 8130 (1996).
[65] M. Büttiker and T. Christen, in *Quantum Transport in Semiconductor Submicron Structures*, edited by B. Kramer (Kluwer Academic Publishers, Dordrecht, 1996).
[66] M. Büttiker, A. Prêtre, and H. Thomas, Z. Phys. B: Conens. Matter **94**, 133 (1994).
[67] V. Gasparian, T. Christen, and M. Büttiker, Phys. Rev. A **54**, 4022 (1996).